Rend. Sem. Mat. Univ. Pol. Torino
Vol. 61, 3 (2003)
Splines and Radial Functions

A. Iske*

RADIAL BASIS FUNCTIONS: BASICS, ADVANCED TOPICS AND MESHFREE METHODS FOR TRANSPORT PROBLEMS

Abstract. This invited contribution first reviews basic features of multivariate interpolation by radial basis functions, before selected of its advanced topics are addressed, including recent results concerning local polyharmonic spline interpolation. The latter is one main ingredient of a novel class of adaptive meshfree semi-Lagrangian methods for transport problems. The construction of these particle-based advection schemes is discussed in detail. Numerical examples concerning meshfree flow simulation are provided.

1. Introduction

Radial basis functions are well-known as traditional and powerful tools for multivariate interpolation from scattered data, see [5, 12, 13, 38, 42] for some different surveys, and [24] for a recent tutorial with accompanying exercises and supplementary software, `www.ma.tum.de/primus2001/radial/`.

Just very recently, radial basis functions have gained enormous popularity in meshfree methods for partial differential equations (PDEs). The theory includes meshfree Galerkin methods [51], collocation methods [16, 17], and multilevel schemes [15]. First applications of radial basis functions in computational fluid dynamics are dating back to Kansa [26, 27]. There is nowadays a vast amount of literature on the subject, see e.g. the rich bibliography in [15, 44]. For a couple of more recent contributions concerning radial basis functions for solving PDEs, we refer to the special issue [56].

This paper first reviews basic features of multivariate interpolation by radial basis functions in the following Section 2, before recent results concerning local polyharmonic spline interpolation are discussed in Section 3. The latter have provided recent advances in the numerical simulation of transport processes by meshfree particle methods [1, 2, 3]. Details on these are explained in Section 4, and numerical examples concerning meshfree flow simulation are finally presented in Section 5.

*This paper is based on an invited lecture which I gave at the workshop *Spline Functions and Radial Functions: Applications to Integral and Differential Problems* of the GNCS, held at the University of Turin in February 2003. I wish to thank the organizers of the meeting for their generous support and their kind hospitality. Moreover, the assistance of Martin Käser with the preparation of the numerical examples is gratefully appreciated.

2. Radial basis function interpolation

2.1. Interpolation scheme

In order to explain multivariate scattered data interpolation by radial basis functions, suppose a data vector $u\big|_\Xi = (u(\xi_1), \ldots, u(\xi_n))^T \in \mathbb{R}^n$ of function values, sampled from an unknown function $u : \mathbb{R}^d \to \mathbb{R}$ at a *scattered* finite point set $\Xi = \{\xi_1, \ldots, \xi_n\} \subset \mathbb{R}^d$, $d \geq 1$, is given. Scattered data interpolation requirescomputing a *suitable* interpolant $s : \mathbb{R}^d \to \mathbb{R}$ satisfying $s\big|_\Xi = u\big|_\Xi$, i.e.,

$$(1) \qquad s(\xi_j) = u(\xi_j), \qquad \text{for all } 1 \leq j \leq n.$$

To this end, the radial basis function interpolation scheme works with a fixed *radial* function $\phi : [0, \infty) \to \mathbb{R}$, and the interpolant s in (1) is assumed to have the form

$$(2) \qquad s(x) = \sum_{j=1}^{n} c_j \phi(\|x - \xi_j\|) + p(x), \qquad p \in \mathcal{P}_m^d,$$

where $\|\cdot\|$ is the Euclidean norm on $\mathbb{R}^d$. Moreover, $\mathcal{P}_m^d$ denotes the linear space containing all real-valued polynomials in d variables of degree at most $m - 1$, where $m \equiv m(\phi)$ is said to be the *order* of the basis function ϕ. We come back to the dependence between m and ϕ later in Subsection 2.4. But let us first give some examples for ϕ.

Classical choices for radial basis functions ϕ, along with their order m, are shown in Table 1, where for any $x \in \mathbb{R}$, the symbol $\lceil x \rceil$ denotes as usual the smallest integer greater than or equal to x. Later in this text, $\lfloor x \rfloor$ denotes the largest integer less than or equal to x.

Among the most popular radial basis functions are the *polyharmonic splines*, which are discussed more detailed in Section 3. This class of radial basis functions includes the *thin plate splines*, where $\phi(r) = r^2 \log(r)$ and $m = 2$, which are particularly suited for interpolation from planar scattered data. Further commonly used radial basis functions are given by the *Gaussians*, $\phi(r) = \exp(-r^2)$, the *multiquadrics*, $\phi(r) = (1 + r^2)^{1/2}$ of order $m = 1$, and the *inverse multiquadrics*, $\phi(r) = (1 + r^2)^{-1/2}$, where $m = 0$. Table 1 gives a more general form for the (inverse) multiquadrics and their corresponding order m.

2.2. Compactly supported radial basis functions

More recent developments [50, 53] have provided a whole family of *compactly supported* radial basis functions. In this case, we have $m = 0$ for their order, and so the polynomial part in (2) is omitted. While the radial basis functions in Table 1 can be used in arbitrary space dimension d, the selection of one *suitable* compactly supported ϕ depends on d, see Table 2. Since the dimension d is known beforehand, this is no severe restriction, as shall be established below.

Table 1: Radial basis functions.

Radial Basis Function	$\phi(r) =$	**Parameters**	**Order**
Polyharmonic Splines	r^{ν}	$\nu > 0, \nu \notin 2\mathbb{N}$	$m = \lceil \nu/2 \rceil$
	$r^{2k}\log(r)$	$k \in \mathbb{N}$	$m = k + 1$
Gaussians	$\exp(-r^2)$		$m = 0$
Multiquadrics	$\left(1 + r^2\right)^{\nu}$	$\nu > 0, \nu \notin \mathbb{N}$	$m = \lceil \nu \rceil$
Inverse Multiquadrics	$\left(1 + r^2\right)^{\nu}$	$\nu < 0$	$m = 0$

To this end, let us further discuss some basics about compactly supported radial basis functions. As to Wendland's functions [50], these are of the form

$$\phi_{d,k}(r) = \begin{cases} p_{d,k}, & \text{for } 0 \le r \le 1, \\ 0, & \text{for } r > 1, \end{cases} \tag{3}$$

where $p_{d,k}$ is a specific univariate polynomial of degree $\lfloor d/2 \rfloor + 3k + 1$, and so the support $\mathrm{supp}(\phi_{d,k})$ of $\phi_{d,k} : [0,\infty) \to \mathbb{R}$ is normalized to the unit interval $[0, 1]$. Moreover, due to Wendland's construction in [50], the basis function $\phi_{d,k}$ has derivatives up to order $2k$, i.e., $\phi_{d,k} \in C^{2k}(\mathbb{R}^d)$. Possible choices for $\phi_{d,k}$ are listed in the following Table 2, where the symbol $\doteq$ denotes equality up to a positive factor, and the *truncated power function* $(\cdot)_+ : \mathbb{R} \to [0,\infty)$ is given by $(x)_+ = x$, for $x > 0$, and $(x)_+ = 0$, for $x \le 0$.

By their construction, Wendland's radial basis functions $\phi_{d,k}$ are *positive definite* on $\mathbb{R}^d$.

DEFINITION 1. *A continuous radial function* $\phi : [0,\infty) \to \mathbb{R}$ *is said to be* positive definite *on* $\mathbb{R}^d$, $\phi \in \mathbf{PD}_d$, *iff for any finite set* $\Xi = \{\xi_1, \ldots, \xi_n\}$, $\Xi \subset \mathbb{R}^d$, *of pairwise distinct points the matrix*

$$\Phi_{\phi,\Xi} = \left(\phi(\|\xi_j - \xi_k\|)\right)_{1 \le j,k \le n} \in \mathbb{R}^{n \times n}$$

is positive definite.

Due to the construction in [53], there exists, for any space dimension d, a positive definite and compactly supported $\phi \in \mathbf{PD}_d$ of the form (3). Remarkably enough,

Table 2: Wendland's compactly supported radial basis functions [50].

Dimension d	**Radial Basis Function**	**Smoothness** $2k$
$d = 1$	$\phi_{1,0} = (1-r)_+$ $\phi_{1,1} \doteq (1-r)_+^3(3r+1)$ $\phi_{1,2} \doteq (1-r)_+^5(8r^2+5r+1)$	C^0 C^2 C^4
$d \leq 3$	$\phi_{3,0} = (1-r)_+^2$ $\phi_{3,1} \doteq (1-r)_+^4(4r+1)$ $\phi_{3,2} \doteq (1-r)_+^6(35r^2+18r+3)$ $\phi_{3,3} \doteq (1-r)_+^8(32r^3+25r^2+8r+1)$	C^0 C^2 C^4 C^6
$d \leq 5$	$\phi_{5,0} = (1-r)_+^3$ $\phi_{5,1} \doteq (1-r)_+^5(5r+1)$ $\phi_{5,2} \doteq (1-r)_+^7(16r^2+7r+1)$	C^0 C^2 C^4

Wendland showed that any basis function $\phi_{d,k}$, constructed in [50] (such as any in Table 2), has minimal degree among all positive definite functions $\phi \in \mathbf{PD}_d \cap C^{2k}(\mathbb{R}^d)$ of the form (3). Moreover, by these properties, $\phi_{d,k}$ in (3) is unique up to a positive constant.

2.3. Well-posedness of the interpolation problem

Now let us turn to the well-posedness of the interpolation problem (1). To this end, we distinguish the case, where $m = 0$ from the one where $m > 0$.

First suppose $m = 0$ for the order of the basis function ϕ, such as for the *Gaussians*, the *inverse multiquadrics* (in Table 1) and *Wendland's functions* (in Table 2). In this case, the interpolant s in (2) has the form

$$s(x) = \sum_{j=1}^{n} c_j \phi(\|x - \xi_j\|). \tag{4}$$

By requiring the n interpolation conditions in (1), the computation of the unknown coefficients $c = (c_1, \ldots, c_n)^T \in \mathbb{R}^n$ of s in (4) amounts to solving the linear equation system

$$\Phi_{\phi,\Xi} \cdot c = u\big|_{\Xi}. \tag{5}$$

Recall that according to Definition 1, the matrix $\Phi_{\phi,\Xi}$ in (5) is guaranteed to be positive definite, provided that $\phi \in \mathbf{PD}_d$. In this case, the system (5) has a unique solution. This in turn implies the well-posedness of the given interpolation problem already.

THEOREM 1. *For $\phi \in \mathbf{PD}_d$, the interpolation problem (1) has a unique solution s of the form (4).*

Now let us turn to the case, where $m > 0$ for the order of ϕ. In this case, the interpolant s in (2) contains a nontrivial polynomial part, yielding q additional degrees of freedom, where $q = \begin{pmatrix} m-1+d \\ d \end{pmatrix}$ is the dimension of the polynomial space $\mathcal{P}_m^d$. These additional degrees of freedom are usually eliminated by requiring the q *moment conditions*

$$\sum_{j=1}^{n} c_j p(\xi_j) = 0, \qquad \text{for all } p \in \mathcal{P}_m^d. \tag{6}$$

Altogether, this amounts to solving the linear system

$$\begin{bmatrix} \Phi_{\phi,\Xi} & \Pi_\Xi \\ \Pi_\Xi^T & 0 \end{bmatrix} \cdot \begin{bmatrix} c \\ d \end{bmatrix} = \begin{bmatrix} u\big|_\Xi \\ 0 \end{bmatrix}, \tag{7}$$

where we let $\Pi_\Xi = \left((\xi_j)^\alpha\right)_{1\le j\le n; |\alpha|<m} \in \mathbb{R}^{n\times q}$, and $d = (d_\alpha)_{|\alpha|<m} \in \mathbb{R}^q$ for the coefficients of the polynomial part in (2). Moreover, for any point $x = (x_1, \ldots, x_d)^T \in \mathbb{R}^d$, and multi-index $\alpha = (\alpha_1, \ldots, \alpha_d) \in \mathbb{N}_0^d$ we let $x^\alpha = x_1^{\alpha_1} \cdot \cdots \cdot x_d^{\alpha_d}$, and $|\alpha| = \alpha_1 + \ldots + \alpha_d$.

In order to analyze the existence and uniqueness of a solution of (7), we first consider its corresponding *homogeneous* system

$$\Phi_{\phi,\Xi} \cdot c + \Pi_\Xi \cdot d = 0, \tag{8}$$

$$\Pi_\Xi^T \cdot c = 0, \tag{9}$$

here split into its interpolation conditions (8) and moment conditions (9). If we multiply the equation (8) from left with c^T, and by using the moment conditions (9), we immediately obtain the identity

$$c^T \cdot \Phi_{\phi,\Xi} \cdot c = 0. \tag{10}$$

Now in order to guarantee the existence of a solution to (8),(9) we require that the matrix $\Phi_{\phi,\Xi} \in \mathbb{R}^{n\times n}$ is, for any set Ξ of interpolation points, *positive definite* on the linear subspace of $\mathbb{R}^d$ containing all vectors $c \in \mathbb{R}^n$ satisfying (9), i.e.,

$$c^T \cdot \Phi_{\phi,\Xi} \cdot c > 0, \qquad \text{for all } c \in \mathbb{R}^n \setminus \{0\} \text{ with } \Pi_\Xi^T c = 0. \tag{11}$$

In this case, the basis function ϕ is said to be *conditionally positive definite*, which deserves the following definition.

DEFINITION 2. *A continuous radial function* $\phi : [0, \infty) \to \mathbb{R}$ *is said to be* conditionally positive definite *of order* m *on* $\mathbb{R}^d$*,* $\phi \in \mathbf{CPD}_d(m)$*, iff (11) holds for all possible choices of finite point sets* $\Xi \subset \mathbb{R}^d$*.*

As shall be established in the following Subsection 2.4, we remark that for every radial basis function ϕ in Table 1, we either have $\phi \in \mathbf{CPD}_d(m)$ or $-\phi \in \mathbf{CPD}_d(m)$, with the corresponding order m given in the last column of Table 1. In either case, we say that m is the *order* of the radial basis function ϕ. Note that every positive definite ϕ, such as for instance any of Wendland's functions in Table 2, is conditionally positive definite of order $m = 0$, and therefore $\mathbf{PD}_d = \mathbf{CPD}_d(0)$.

Now let us return to the above discussion concerning the solvability of the linear system (8),(9). With assuming $\phi \in \mathbf{CPD}_d(m)$ (or $-\phi \in \mathbf{CPD}_d(m)$), we conclude $c = 0$ directly from (10), and so (8) becomes $\Pi_\Xi \cdot d = 0$. Therefore, in order to guarantee a unique solution of (8),(9), it remains to require the *injectivity* of the matrix Π_Ξ. But this property depends on the geometry of the interpolation points in Ξ. Indeed, note that the matrix Π_Ξ is injective, iff for $p \in \mathcal{P}_m^d$ the implication

$$p(\xi_j) = 0 \quad \text{for } 1 \le j \le n \qquad \Longrightarrow \qquad p \equiv 0 \tag{12}$$

holds. In this case, any polynomial in $\mathcal{P}_m^d$ can uniquely be reconstructed from its function values sampled at the points in Ξ. The point set Ξ is then said to be $\mathcal{P}_m^d$*-unisolvent*. Note that the requirement (12) for the points in Ξ is rather weak. Indeed, when $m = 0$, the condition is empty, for $m = 1$ it is trivial, and for $m = 2$ the points in Ξ must not lie on a straight line.

We summarize the discussion of this subsection as follows.

THEOREM 2. *For* $\phi \in \mathbf{CPD}_d(m)$*, the interpolation problem (1) has under constraints (6) a unique solution* s *of the form (2), provided that the interpolation points in* Ξ *are* $\mathcal{P}_m^d$*-unisolvent by satisfying (12).*

2.4. Conditionally positive definite functions

By the discussion in the previous subsection, radial basis function interpolation essentially relies on the conditional positive definiteness the chosen basis function ϕ. Indeed, this is one of the key properties of the interpolation scheme. In this subsection, we discuss two alternative ways for the construction and characterization of conditionally positive definite functions.

One technique, dating back to Micchelli [35], works with *completely monotone functions*. The other alternative relies on *generalized Fourier transforms* [23]. We do not intend to discuss these two different techniques in all details. Instead of this we briefly review relevant results. For a more comprehensive discussion concerning conditionally positive definite functions, we refer to the recent survey [45].

Completely monotone functions

DEFINITION 3. *A function* $\psi \in C^{\infty}(0,\infty)$ *is said to be* completely monotone *on* $(0,\infty)$*, iff*

$$(-1)^{\ell}\psi^{\ell}(r) \geq 0, \qquad \ell = 0, 1, 2, \ldots,$$

holds for all $r \in (0,\infty)$.

Micchelli provides in [35] a sufficient criterion for $\phi \in \mathbf{CPD}_d(m)$, which generalizes an earlier result by Schoenberg [47, 48] for positive definite radial functions. Micchelli also conjectured the necessity of this criterion. This was finally shown by Guo, Hu and Sun in [20]. We summarize the relevant results from [20, 35, 47, 48] by

THEOREM 3. *Let* $\phi : [0,\infty) \to \mathbb{R}$ *be a continuous radial function. Moreover, let* $\phi_{\sqrt{}} \equiv \phi(\sqrt{\cdot})$*. Suppose* $\phi_m \equiv (-1)^m \phi_{\sqrt{}}^{(m)}$ *is well-defined and* ϕ_m *is not constant. Then, the following two statements are equivalent.*

(a) $\phi \in \mathbf{CPD}_d(m)$ *for all* $d \geq 1$*;*

(b) ϕ_m *is completely monotone on* $(0,\infty)$.

Now, by using Theorem 3, it is easy to show for any ϕ in Table 1 that either ϕ or $-\phi$ is conditionally positive definite of order m, with m given in the last column of Table 1. Note, however, that the characterization in Theorem 3 applies to *radial* functions only. Moreover, it excludes the construction of *compactly supported* radial basis functions. The latter is due to the Bernstein-Widder theorem [4] (see also [52]) which says that any function $\psi : [0,\infty) \to \mathbb{R}$ is completely monotone on $(0,\infty)$, if and only if it has a Laplace-Stieltjes-type representation of the form

$$\psi(r) = \int_0^{\infty} \exp(-rs)\, d\mu(s),$$

where μ is monotonically increasing with $\int_0^{\infty} d\mu(s) < \infty$. Hence, in this case ψ has no zero, and so any $\psi = \phi_m$ in (b) of Theorem 3 cannot be compactly supported.

Generalized Fourier transforms

A different technique for the characterization and construction of (not necessarily radial) functions $\phi \in \mathbf{CPD}_d(m)$, including compactly supported ones, is using (generalized) Fourier transforms, see the recent survey [45, Section 4] (which basically relies on the results in [23]). We do not explain generalized Fourier transforms here, but rather refer to the textbooks [18, 19], where a comprehensive treatment of the relevant technical background is provided.

For the purposes in this subsection, it is sufficient to say that every radial basis function ϕ in Table 1 has a *radial* (generalized) Fourier transform $\hat{\phi} \in C(0,\infty)$ satisfying the following two properties.

- $\hat{\phi}(\|\cdot\|)$ is L_1-integrable around infinity, i.e.,

$$\int_{\mathbb{R}^d\setminus B_1(0)} \left|\hat{\phi}(\|\omega\|)\right| d\omega < \infty, \tag{13}$$

- $\hat{\phi}(\|\cdot\|)$ has at most an algebraic singularity of *order* $s_0 \in \mathbb{N}_0$ at the origin, such that

$$\int_{B_1(0)} \|\omega\|^{s_0}\hat{\phi}(\|\omega\|)\, d\omega < \infty, \tag{14}$$

holds, with $s_0 \in \mathbb{N}_0$ being minimal in (14).

Table 3 shows the (generalized) Fourier transforms of the radial basis functions in Table 1, along with their order s_0, where $\doteq$ means equality up to a constant factor, and where K_δ denotes the modified Bessel function.

We remark that if ϕ has a Fourier transform $\hat{\phi} \in L_1(\mathbb{R}^d)$,

$$\hat{\phi}(\|\omega\|) = \int_{\mathbb{R}^d} \phi(\|x\|) \exp(-ix^T\omega)\, dx,$$

in the classical sense, then this *classical* Fourier transform $\hat{\phi}$ coincides with the generalized Fourier transform of ϕ. Examples are given by the Gaussians, the inverse multiquadrics, and Wendland's compactly supported radial basis functions. In this case, we have $s_0 = 0$ for the order of $\hat{\phi}$.

Now let us turn straight to the characterization of conditionally positive definite functions by generalized Fourier transforms. This particular characterization relies on the identity

$$\sum_{j,k=1}^{n} c_j c_k \phi(\|\xi_j - \xi_k\|) = (2\pi)^{-d} \int_{\mathbb{R}^d} \hat{\phi}(\|\omega\|) \left|\sum_{j=1}^{n} c_j \exp(-i\xi_j^T\omega)\right|^2 d\omega, \tag{15}$$

which can be established [23] for any $\hat{\phi}$ satisfying (13) and (14), provided that the *symbol function*

$$\sigma_{c,\Xi}(\omega) = \sum_{j=1}^{n} c_j \exp(-i\xi_j^T\omega) \tag{16}$$

has a zero at the origin of order at least $m = \lceil s_0/2\rceil$. Note that the latter can be guaranteed by requiring the moment conditions (6) with $m = \lceil s_0/2\rceil$.

THEOREM 4. *A continuous radial function $\phi : [0,\infty) \to \mathbb{R}$ is conditionally positive definite on $\mathbb{R}^d$, if ϕ has a continuous nonnegative generalized Fourier transform $\hat{\phi} \not\equiv 0$ satisfying (13) and (14). In this case, we have $m = \lceil s_0/2\rceil$ for the order of $\phi \in$ **CPD**$_d(m)$.*

Proof. Let $\hat{\phi}$ satisfy (13) and (14), and suppose (6) with $m = \lceil s_0/2 \rceil$, so that the identity (15) holds. By the nonnegativity of $\hat{\phi}$, the quadratic form

$$c^T \Phi_{\phi,\Xi} c = \sum_{j,k=1}^{n} c_j c_k \phi(\|\xi_j - \xi_k\|)$$

appearing in the left hand side of (15), is nonnegative. Hence it remains to show that $c^T \Phi_{\phi,\Xi} c$ vanishes, if and only if $c = 0$. In order to see this, suppose that $c^T \Phi_{\phi,\Xi} c$, and thus the right hand side in (15), vanishes. In this case, the symbol function $\sigma_{c,\Xi}$ in (16) must vanish on an open subset of $\mathbb{R}^d$ with nonempty interior. But then, due to the analyticity of $\sigma_{c,\Xi}$, this implies that the symbol function vanishes identically on $\mathbb{R}^d$, i.e., $\sigma_{c,\Xi} \equiv 0$. Since the points in Ξ are pairwise distinct, and so the exponentials $\exp(-i\xi_j^T \omega)$ are linearly independent, the latter is true, if and only if $c = 0$.

□

Table 3: Generalized Fourier transforms of radial basis functions.

Radial Basis Function	$\phi(r) =$	$\hat{\phi}(s) \doteq$	**Order** s_0
Polyharmonic Splines	r^ν	$s^{-d-\nu}$	$\lfloor \nu \rfloor + 1$
	$r^{2k}\log(r)$	s^{-d-2k}	$2k + 1$
Gaussians	$\exp(-r^2)$	$\exp(-s^2/4)$	0
Multiquadrics	$\left(1 + r^2\right)^\nu$	$K_{d/2+\nu}(s) \cdot s^{-(d/2+\nu)}$	$\lfloor 2\nu \rfloor + 1$
Inverse Multiquadrics	$\left(1 + r^2\right)^\nu$	$K_{d/2+\nu}(s) \cdot s^{-(d/2+\nu)}$	0

2.5. Error estimates in native function spaces

This subsection is devoted to available bounds on the error $\|u - s_{u,\Xi}\|_{L_\infty(\Omega)}$, where $\Omega \subset \mathbb{R}^d$ is a bounded and open domain comprising Ξ, i.e., $\Xi \subset \Omega$. Moreover, it is assumed that $\Omega \subset \mathbb{R}^d$ satisfies an *interior cone condition*, and u lies in the *native function space* $\mathcal{F}_\phi$ associated with the radial basis function $\phi \in \mathbf{CPD}_d(m)$.

In order to explain the native function space $\mathcal{F}_\phi$ just very briefly, let

$$\mathcal{R}_\phi = \left\{ s_{c,p,\Xi} = \sum_{\xi\in\Xi} c_\xi \phi(\|\cdot - \xi\|) + p : \Xi \subset \mathbb{R}^d \text{ finite }, \Pi_\Xi^T c = 0,\, p \in \mathcal{P}_m^d \right\}$$

denote the *recovery space* of $\phi \in \mathbf{CPD}_d(m)$ containing all possible interpolants of the form (2). Due to its conditional positive definiteness, ϕ provides by

$$(s_{c,p,\Xi}, s_{d,q,\Upsilon})_\phi = \sum_{\xi\in\Xi,\upsilon\in\Upsilon} c_\xi d_\upsilon \phi(\|\xi - \upsilon\|), \qquad \text{for } s_{c,p,\Xi}, s_{d,q,\Upsilon} \in \mathcal{R}_\phi,$$

a semi-inner product $(\cdot,\cdot)_\phi$, and semi-norm $|\cdot|_\phi = (\cdot,\cdot)_\phi^{1/2}$, whose kernel are the polynomials in $\mathcal{P}_m^d$. The topological closure of the linear space $(\mathcal{R}_\phi, |\cdot|_\phi)$ is the native function space $\mathcal{F}_\phi$, i.e., $\overline{\mathcal{R}_\phi} = \mathcal{F}_\phi$.

One key feature of the radial basis function interpolation scheme is its *optimal recovery*, which can be explained as follows. For $u \in \mathcal{F}_\phi$ and any finite point set $\Xi \subset \mathbb{R}^d$, the interpolant $s_{u,\Xi}$ satisfying $s_{u,\Xi}\big|_\Xi = u\big|_\Xi$ is the orthogonal projection of u onto the recovery space $\mathcal{R}_\phi \subset \mathcal{F}_\phi$, so that the *Pythagoras theorem*

$$|s_{u,\Xi}|_\phi^2 + |u - s_{u,\Xi}|_\phi^2 = |u|_\phi^2, \qquad \text{for } u \in \mathcal{F}_\phi,$$

holds. Hence, by

$$|s_{u,\Xi}|_\phi^2 \le |u|_\phi^2, \qquad \text{for } u \in \mathcal{F}_\phi,$$

the interpolation process is *optimal* w.r.t. the *optimal recovery space* $\mathcal{F}_\phi$. For more details on this, we refer to the variational theory in the seminal papers by Madych & Nelson [29, 30, 31].

Now let us turn to error estimates. For the radial basis functions in Table 1, available bounds on the pointwise error $\epsilon_x = u(x) - s(x)$, $x \in \Omega$, are due to [30, 31, 54] of the form

$$|u(x) - s_{u,\Xi}(x)| \le C \cdot |u|_\phi \cdot F_\phi^{1/2}(h_{\varrho,\Xi}(x)), \qquad \text{for } u \in \mathcal{F}_\phi, \tag{17}$$

where, for some specific radius $\varrho > 0$, the *local fill distance*

$$h_{\varrho,\Xi}(x) = \max_{y\in B_\varrho(x)} \min_{\xi\in\Xi} \|y - \xi\|$$

reflects the local density of Ξ around x, where $B_\varrho(x) = \{y : \|y - x\| \le \varrho\}$. Moreover, $F_\phi : [0,\infty) \to [0,\infty)$ is a monotonically increasing function with $F_\phi(0) = 0$, which depends merely on ϕ. For the radial basis functions ϕ in Table 1, its corresponding F_ϕ is listed in Table 4, see also [42].

It can be shown that the given pointwise error bounds carry over to uniform bounds in the domain Ω, yielding error estimates depending on the *fill distance*

$$h_{\Xi,\Omega} = \max_{y\in\Omega} \min_{\xi\in\Xi} \|y - \xi\| \tag{18}$$

Table 4: Radial basis functions: Convergence Rates (see [42] for details).

Radial Basis Function	$\phi(r) =$	$F_\phi(h) \doteq$
Polyharmonic Splines	r^ν	h^ν
	$r^{2k}\log(r)$	h^{2k}
Gaussians	$\exp(-r^2)$	$\exp(-\alpha/h)$
(Inverse) Multiquadrics	$\left(1+r^2\right)^\nu$	$\exp(-\alpha/h)$

of Ξ in Ω, i.e.,

$$\|u - s_{u,\Xi}\|_{L_\infty(\Omega)} \le C \cdot |u|_\phi \cdot F_\phi^{1/2}(h_{\Xi,\Omega}), \qquad \text{for } u \in \mathcal{F}_\phi. \tag{19}$$

For further details, we refer to [42, 46].

2.6. Lagrange representation of the interpolant

In the following discussion of this paper, especially in the following Section 3, it is convenient to work with the *Lagrange representation*

$$s_{u,\Xi}(x) = \sum_{j=1}^{n} \lambda_j(x) u(\xi_j) \tag{20}$$

of the interpolant $s \equiv s_{u,\Xi}$ in (2), where the *Lagrange basis functions* $\lambda_1(x), \ldots, \lambda_n(x)$ satisfy

$$\lambda_j(\xi_k) = \begin{cases} 1, & \text{for } j = k, \\ 0, & \text{for } j \neq k \end{cases} \qquad 1 \le j, k \le n, \tag{21}$$

and so $s\big|_\Xi = u\big|_\Xi$.

For a fixed $x \in \mathbb{R}^d$, the vectors

$$\lambda(x) = (\lambda_1(x), \ldots, \lambda_n(x))^T \in \mathbb{R}^n \quad \text{and} \quad \mu(x) = (\mu_1(x), \ldots, \mu_q(x))^T \in \mathbb{R}^q$$

are the unique solution of the linear system

$$\begin{bmatrix} \Phi_{\phi,\Xi} & \Pi_\Xi \\ \Pi_\Xi^T & 0 \end{bmatrix} \cdot \begin{bmatrix} \lambda(x) \\ \mu(x) \end{bmatrix} = \begin{bmatrix} \varphi(x) \\ \pi(x) \end{bmatrix}, \tag{22}$$

where $\varphi(x) = (\phi(\|x - \xi_j\|))_{1 \le j \le n} \in \mathbb{R}^n$ and $\pi(x) = (x^\alpha)_{|\alpha|<m} \in \mathbb{R}^q$. We abbreviate this linear system as

$$A \cdot \nu(x) = \beta(x)$$

by letting

$$A = \begin{bmatrix} \Phi_{\phi,\Xi} & \Pi_\Xi \\ \Pi_\Xi^T & 0 \end{bmatrix}, \quad \nu(x) = \begin{bmatrix} \lambda(x) \\ \mu(x) \end{bmatrix}, \quad \beta(x) = \begin{bmatrix} \varphi(x) \\ \pi(x) \end{bmatrix}.$$

This allows us to combine the two alternative representations for s in (20) and (2) by

$$\begin{aligned} s(x) &= < \lambda(x), u\big|_\Xi > \\ &= < \nu(x), u_\Xi > \\ &= < A^{-1} \cdot \beta(x), u_\Xi > \\ &= < \beta(x), A^{-1} \cdot u_\Xi > \\ &= < \beta(x), b >, \end{aligned} \tag{23}$$

where $< \cdot, \cdot >$ denotes the inner product of the Euclidean space $\mathbb{R}^d$, and where we let

$$u_\Xi = \begin{bmatrix} u\big|_\Xi \\ 0 \end{bmatrix} \in \mathbb{R}^{n+q} \quad \text{and} \quad b = \begin{bmatrix} c \\ d \end{bmatrix} \in \mathbb{R}^{n+q}$$

for the right hand side and the solution of the linear system (7).

3. Polyharmonic spline interpolation

In this section, details on the interpolation by *polyharmonic splines*, often also referred to as *surface splines*, are explained. The utility of polyharmonic splines for multivariate interpolation was established by Duchon [8, 9, 10]. In order to discuss the particular setting of Duchon, let us be more specific about the choice of the basis function ϕ. According to [8, 9, 10], we assume from now the form

$$\phi_{d,k}(r) = \begin{cases} r^{2k-d} \log(r), & \text{for } d \text{ even}, \\ r^{2k-d}, & \text{for } d \text{ odd}, \end{cases}$$

for the polyharmonic splines, where k is required to satisfy $2k > d$. According to Table 1 (last column), the order of $\phi_{d,k}$ is given by $m = k - \lceil d/2 \rceil + 1$.

Now note that the inclusion $\mathbf{CPD}_d(m_1) \subset \mathbf{CPD}_d(m_2)$, for $m_1 \le m_2$, allows us to also work with any order greater than m. In order to comply with Duchon's setting, we replace the *minimal* choice $m = k - \lceil d/2 \rceil + 1$ by $k \ge m$. Therefore, we let from now $m = k$ for the order of $\phi_{d,k} \in \mathbf{CPD}_d(m)$. We come back with an explanation concerning this particular choice for m later in Subsection 3.1.

With using $m = k$, the resulting interpolant in (2) has the form

$$s(x) = \sum_{i=1}^{n} c_i \phi_{d,k}(\|x - \xi_i\|) + \sum_{|\alpha|<k} d_\alpha x^\alpha. \tag{24}$$

We remark that the polyharmonic spline $\phi_{d,k}$ is the fundamental solution of the k-th iterated Laplacian, i.e.,

$$\Delta^k \phi_{d,k}(\|x\|) = c\delta_x.$$

For instance, for $d = k = 2$, the thin plate spline $\phi_{2,2}(r) = r^2 \log(r)$ solves the *biharmonic equation*

$$\Delta\Delta\phi_{2,2}(\|x\|) = c\delta_x.$$

In this case, the interpolant s in (24) has the form

$$s(x) = \sum_{i=1}^{n} c_i \|x - \xi_i\|^2 \log(\|x - \xi_i\|) + d_1 + d_2 x_1 + d_3 x_2, \tag{25}$$

where we let $x = (x_1, x_2)^T \in \mathbb{R}^2$. Finally, we remark that for the univariate case, where $d = 1$, the polyharmonic spline $\phi_{1,k} = r^{2k-1}$, $k \geq 1$, coincides with the *natural spline* of order $2k$.

3.1. Optimal recovery in Beppo-Levi spaces

Recall the discussion in Subsection 2.5 concerning optimal recovery of radial basis function interpolation in native function spaces. In this subsection, we wish to discuss the native function space of polyharmonic splines.

Due to fundamental results in the seminal papers [8, 9, 10] of Duchon and [32, 33, 34] of Meinguet, for a fixed finite point set $\Xi \subset \mathbb{R}^d$, an interpolant s in (24) minimizes the energy

$$|u|^2_{\mathrm{BL}^k(\mathbb{R}^d)} = \int_{\mathbb{R}^d} \sum_{|\alpha|=k} \binom{k}{\alpha} \left(D^\alpha u\right)^2 \, dx, \qquad \binom{k}{\alpha} = \frac{k!}{\alpha_1! \cdot \cdots \cdot \alpha_d!}, \tag{26}$$

among all functions u of the *Beppo-Levi space*

$$\mathrm{BL}^k(\mathbb{R}^d) = \left\{ u \in C(\mathbb{R}^d) : D^\alpha u \in L^2(\mathbb{R}^d) \text{ for all } |\alpha| = k \right\} \subset C(\mathbb{R}^d)$$

satisfying $u\big|_\Xi = s\big|_\Xi$. So the Beppo-Levi space $\mathrm{BL}^k(\mathbb{R}^d)$ is equipped with the semi-norm $|\cdot|_{\mathrm{BL}^k(\mathbb{R}^d)}$, whose kernel is the polynomial space $\mathcal{P}_k^d$. The latter explains why we use order $m = k$ rather than the *minimal* choice $m = k - \lceil d/2 \rceil + 1$. In this case, the Beppo-Levi space $\mathrm{BL}^k(\mathbb{R}^d)$ is the *optimal recovery space* $\mathcal{F}_\phi$ for the polyharmonic splines $\phi_{d,k}$. Note that $\mathrm{BL}^k(\mathbb{R}^d)$ is the Sobolev space $H^k(\mathbb{R}^d)$.

When working with thin plate splines, $\phi_{2,2}(r) = r^2 \log(r)$, in two dimensions we have

$$|u|^2_{\mathrm{BL}^2(\mathbb{R}^2)} = \int_{\mathbb{R}^2} \left(u^2_{x_1x_1} + 2u^2_{x_1x_2} + u^2_{x_2x_2} \right) dx_1\, dx_2, \quad \text{for } u \in \mathrm{BL}^2(\mathbb{R}^2).$$

In this case, the semi-norm $|\cdot|_{\mathrm{BL}^2(\mathbb{R}^2)}$ is the *bending energy* of a thin plate of infinite extent, and this explains the naming of *thin plate splines*.

3.2. Approximation order

The following result concerning the convergence rate of polyharmonic spline interpolation is dating back to Wu & Schaback [54] (cf. Subsection 2.5).

THEOREM 5. *Let Ω be a bounded and open domain satisfying an interior cone condition. Then, there exist constants h_0, C, such that for any finite point set $\Xi \subset \Omega$ satisfying $h_{\Xi,\Omega} \le h_0$ and any function $u \in \mathrm{BL}^k(\mathbb{R}^d)$ the error bound*

$$\|u - s\|_{L_\infty(\Omega)} \le C \cdot |u|_{\mathrm{BL}^k(\mathbb{R}^d)} h^{k-d/2}_{\Xi,\Omega}$$

holds, where s is the polyharmonic spline interpolant in (24), using $\phi_{d,k}$, satisfying $s\big|_\Xi = u\big|_\Xi$.

Hence, in this sense, the *global* approximation order of the polyharmonic spline interpolation scheme, using $\phi_{d,k}$, is $p = k - d/2$ with respect to the Beppo-Levi space $\mathrm{BL}^k(\mathbb{R}^d)$.

In the following discussion of this subsection, we analyze the approximation order of *local* polyharmonic spline interpolation. We remark that this analysis in combination with the subsequent discussion concerning the stability of local polyharmonic spline interpolation is relevant for the application in the following Section 4.

As regards the local approximation order, we consider solving, for some fixed point $\xi_0 \in \mathbb{R}^d$ and any $h > 0$, the interpolation problem

$$u(\xi_0 + h\xi_j) = s^h(\xi_0 + h\xi_j), \quad 1 \le j \le n, \tag{27}$$

where $\Xi = \{\xi_1, \ldots, \xi_n\} \subset \mathbb{R}^d$ is a $\mathcal{P}^d_k$-unisolvent point set of *moderate* size, i.e., n is small. Moreover, s^h denotes the unique polyharmonic spline interpolant of the form

$$s^h(hx) = \sum_{j=1}^n c^h_j \phi_{d,k}(\|hx - h\xi_j\|) + \sum_{|\alpha|<k} d^h_\alpha (hx)^\alpha \tag{28}$$

satisfying (27). The discussion in this subsection is dominated by the following definition.

DEFINITION 4. *Let s^h denote the polyharmonic spline interpolant, using $\phi_{d,k}$, satisfying (27). We say that the* approximation order *of local polyharmonic spline interpolation at $\xi_0 \in \mathbb{R}^d$ and with respect to the function space $\mathcal{F}$ is p, iff for any $u \in \mathcal{F}$ the* *asymptotic bound*

$$|u(\xi_0 + hx) - s^h(\xi_0 + hx)| = \mathcal{O}(h^p), \quad h \to 0,$$

holds for any $x \in \mathbb{R}^d$*, and any finite* $\mathcal{P}_k^d$*-unisolvent point set* $\Xi \subset \mathbb{R}^d$.

For the sake of notational simplicity, we let from now $\xi_0 = 0$, which is, due to the shift-invariance of the interpolation scheme, without loss of generality.

Note that the coefficients $c^h = (c_1^h, \dots, c_n^h)^T \in \mathbb{R}^n$, $d^h = (d_\alpha^h)_{|\alpha|<k} \in \mathbb{R}^q$ of (28) are solving the linear system

$$\begin{bmatrix} \Phi_h & \Pi_h \\ \Pi_h^T & 0 \end{bmatrix} \cdot \begin{bmatrix} c^h \\ d^h \end{bmatrix} = \begin{bmatrix} u\big|_{h\Xi} \\ 0 \end{bmatrix}, \tag{29}$$

where we let

$$\begin{aligned} \Phi_h &= \left(\phi_{d,k}(\|h\xi_i - h\xi_j\|\right)_{1\le i,j\le n} \in \mathbb{R}^{n\times n}, \\ \Pi_h &= \left((h\xi_i)^\alpha\right)_{1\le i\le n;|\alpha|<k} \in \mathbb{R}^{n\times q}, \\ u\big|_{h\Xi} &= (u(h\xi_i))_{1\le i\le n} \in \mathbb{R}^n. \end{aligned}$$

We abbreviate the above linear system (29) as

$$A_h \cdot b^h = u_h, \tag{30}$$

i.e., for notational brevity, we let

$$A_h = \begin{bmatrix} \Phi_h & \Pi_h \\ \Pi_h^T & 0 \end{bmatrix}, \quad b^h = \begin{bmatrix} c^h \\ d^h \end{bmatrix}, \quad \text{and} \quad u_h = \begin{bmatrix} u\big|_{h\Xi} \\ 0 \end{bmatrix}.$$

Recall from the discussion in Subsection 2.6 that any interpolant s^h satisfying (27) has a Lagrange-type representation of the form

$$s^h(hx) = \sum_{i=1}^n \lambda_i^h(hx)u(h\xi_i), \tag{31}$$

corresponding to the one in (20), where moreover

$$\sum_{i=1}^n \lambda_i^h(hx)p(h\xi_i) = p(hx), \quad \text{for all } p \in \mathcal{P}_k^d, \tag{32}$$

due to the reconstruction of polynomials in $\mathcal{P}_k^d$.

Moreover, for $x \in \mathbb{R}^d$, the vector $\lambda^h(hx) = (\lambda_1^h(hx), \dots, \lambda_n^h(hx))^T \in \mathbb{R}^n$ is, together with $\mu^h(hx) = (\mu_\alpha^h(hx))_{|\alpha|<k} \in \mathbb{R}^q$, the unique solution of the linear system

$$\begin{bmatrix} \Phi_h & \Pi_h \\ \Pi_h^T & 0 \end{bmatrix} \cdot \begin{bmatrix} \lambda^h(hx) \\ \mu^h(hx) \end{bmatrix} = \begin{bmatrix} \varphi_h(hx) \\ \pi_h(hx) \end{bmatrix}, \tag{33}$$

where

$$\begin{aligned} \Phi_h &= \left(\phi_{d,k}(\|h\xi_i - h\xi_j\|)\right)_{1\le i,j\le n} \in \mathbb{R}^{n\times n}, \\ \Pi_h &= \left((h\xi_i)^\alpha\right)_{1\le i\le n;|\alpha|<k} \in \mathbb{R}^{n\times q}, \\ \varphi_h(hx) &= \left(\phi_{d,k}(\|hx - h\xi_j\|)\right)_{1\le j\le n} \in \mathbb{R}^n, \\ \pi_h(hx) &= \left((hx)^\alpha\right)_{|\alpha|<k} \in \mathbb{R}^q. \end{aligned}$$

It is convenient to abbreviate the system (33) as $A_h \cdot \nu^h(hx) = \beta_h(hx)$, i.e., we let

$$A_h = \begin{bmatrix} \Phi_h & \Pi_h \\ \Pi_h^T & 0 \end{bmatrix}, \quad \nu^h(hx) = \begin{bmatrix} \lambda^h(hx) \\ \mu^h(hx) \end{bmatrix}, \quad \beta_h(hx) = \begin{bmatrix} \varphi_h(hx) \\ \pi_h(hx) \end{bmatrix}.$$

Starting with the Lagrange representation of s^h in (31), we obtain

$$\begin{aligned} s^h(hx) &= \;< \lambda^h(hx), u\big|_{h\Xi} > \\ &= \;< \nu^h(hx), u_h > \\ &= \;< A_h^{-1} \cdot \beta_h(hx), u_h > \\ &= \;< \beta_h(hx), A_h^{-1} \cdot u_h > \\ &= \;< \beta_h(hx), b_h >, \end{aligned} \tag{34}$$

see the identity (23). This in particular combines the two alternative representations for s^h in (31) and (28).

The following lemma, proven in [25], plays a key role in the following discussion. It states that the Lagrange basis of the polyharmonic spline interpolation scheme is invariant under uniform scalings. As established in the recap of the proof from [25] below, this result mainly relies on the (generalized) homogeneity of $\phi_{d,k}$.

LEMMA 1. *For any $h > 0$, let $\lambda^h(hx)$ be the solution in (33). Then,*

$$\lambda^h(hx) = \lambda^1(x), \qquad \textit{for every } x \in \mathbb{R}^d.$$

Proof. For fixed $\Xi = \{\xi_1, \dots, \xi_n\} \subset \mathbb{R}^d$, and any $h > 0$, let

$$\mathcal{R}_{\phi,\Xi}^h = \left\{ \sum_{i=1}^n c_i \phi_{d,k}(\|\cdot - h\xi_i\|) + p : p \in \mathcal{P}_k^d, \sum_{i=1}^n c_i q(\xi_i) = 0 \text{ for all } q \in \mathcal{P}_k^d \right\}$$

denote the space of all possible polyharmonic spline interpolants of the form (28) satisfying (27). In what follows, we show that $\mathcal{R}^h_{\phi,\Xi}$ is a scaled version of $\mathcal{R}^1_{\phi,\Xi}$, so that $\mathcal{R}^h_{\phi,\Xi} = \left\{\sigma_h(s) : s \in \mathcal{R}^1_{\phi,\Xi}\right\}$, where the dilatation operator σ_h is given by $\sigma_h(s) = s(\cdot/h)$. This then implies that, due to the unicity of the interpolation in either space, $\mathcal{R}^h_{\phi,\Xi}$ or $\mathcal{R}^1_{\phi,\Xi}$, their Lagrange basis functions must coincide by satisfying $\lambda^h = \sigma_h(\lambda^1)$, as stated above.

In order to show that $\mathcal{R}^h_{\phi,\Xi} = \sigma_h(\mathcal{R}^1_{\phi,\Xi})$, we distinguish the special case where d is even from the one where d is odd. If the space dimension d is odd, then $\mathcal{R}^h_{\phi,\Xi} = \sigma_h(\mathcal{R}^1_{\phi,\Xi})$ follows immediately from the homogeneity of $\phi_{d,k}$, where $\phi_{d,k}(hr) = h^{2k-d}\phi_{d,k}(r)$.

Now suppose that d is even. In this case we have

$$\phi_{d,k}(hr) = h^{2k-d}\left(\phi_{d,k}(r) + r^{2k-d}\log(h)\right).$$

Therefore, any function $s^h \in \mathcal{R}^h_{\phi,\Xi}$ has, for some $p \in \mathcal{P}^d_k$, the form

$$s^h(hx) = h^{2k-d}\left(\sum_{i=1}^{n} c_i^h \phi_{d,k}(\|x - \xi_i\|) + \log(h)q(x)\right) + p(x),$$

where we let

$$q(x) = \sum_{i=1}^{n} c_i^h \|x - \xi_i\|^{2k-d}.$$

In order to see that s^h is contained in $\sigma_h(\mathcal{R}^1_{\phi,\Xi})$, it remains to show that the degree of the polynomial q is at most $k-1$. To this end, we rewrite q as

$$q(x) = \sum_{i=1}^{n} c_i^h \sum_{|\alpha|+|\beta|=2k-d} c_{\alpha,\beta} \cdot x^\alpha (\xi_i)^\beta = \sum_{|\alpha|+|\beta|=2k-d} c_{\alpha,\beta} \cdot x^\alpha \sum_{i=1}^{n} c_i^h (\xi_i)^\beta,$$

for some coefficients $c_{\alpha,\beta} \in \mathbb{R}$ with $|\alpha| + |\beta| = 2k - d$. Due to the vanishing moment conditions

$$\sum_{i=1}^{n} c_i^h p(h\xi_i) = 0, \qquad \text{for all } p \in \mathcal{P}^d_k,$$

for the coefficients $c_1^h, \ldots, c_n^h$, this implies that the degree of q is at most $2k - d - k = k - d < k$. Therefore, $s^h \in \sigma_h(\mathcal{R}^1_{\phi,\Xi})$, and so $\mathcal{R}^h_{\phi,\Xi} \subset \sigma_h(\mathcal{R}^1_{\phi,\Xi})$. The inclusion $\mathcal{R}^1_{\phi,\Xi} \subset \sigma_h^{-1}(\mathcal{R}^h_{\phi,\Xi})$ can be proven accordingly.

Altogether, we find that $\mathcal{R}^h_{\phi,\Xi} = \sigma_h(\mathcal{R}^1_{\phi,\Xi})$ for any d, which completes our proof. □

Now let us draw important conclusions on the approximation order of local polyharmonic spline interpolation with respect to C^k. To this end, regard for $u \in C^k$, any

$x \in \mathbb{R}^d$ and $h > 0$, the k-th order Taylor polynomial

$$p^h(y) = \sum_{|\alpha|<k} \frac{1}{\alpha!} D^\alpha u(hx)(y - hx)^\alpha. \tag{35}$$

By using

$$u(hx) = p^h(h\xi_i) - \sum_{0<|\alpha|<k} \frac{1}{\alpha!} D^\alpha u(hx)(h\xi_i - hx)^\alpha, \qquad \text{for all } 1 \le i \le n,$$

in combination with (31) and (32), we obtain the identity

$$u(hx) - s^h(hx) = \sum_{i=1}^n \lambda_i^h(hx) \left[p^h(h\xi_i) - u(h\xi_i) \right].$$

Now due to Lemma 1, the *Lebesgue constant*

$$\Lambda = \sup_{h>0} \sum_{i=1}^n \left| \lambda_i^h(hx) \right| = \sum_{i=1}^n \left| \lambda_i^1(x) \right|$$

is bounded, locally around the origin $\xi_0 = 0$, and therefore we can conclude

$$|u(hx) - s^h(hx)| = \mathcal{O}(h^k), \qquad h \to 0.$$

Altogether, this yields the following result.

THEOREM 6. *The approximation order of local polyharmonic spline interpolation, using $\phi_{d,k}$, with respect to C^k is $p = k$.*

We remark that the above Theorem 6 generalizes a previous result in [21] concerning the local approximation order of thin plate spline interpolation in the plane.

COROLLARY 1. *The approximation order of local thin plate spline interpolation, using $\phi_{2,2} = r^2 \log(r)$, with respect to C^2 is $p = 2$.*

3.3. Numerical stability

This section is devoted to the construction of a numerically stable algorithm for the evaluation of polyharmonic spline interpolants. Recall that the stability of an algorithm always depends on the conditioning of the given problem. For a more general discussion on the relevant principles and concepts from error analysis, especially the *condition number* of a given *problem* versus the *stability* of a *numerical algorithm*, we recommend the textbook [22].

In order to briefly explain the conditioning of polyharmonic spline interpolation, let $\Omega \subset \mathbb{R}^d$ denote a compact domain comprising $\Xi = \{\xi_1, \ldots, \xi_n\}$, i.e., $\Xi \subset \Omega$, the

$\mathcal{P}_k^d$-unisolvent set of interpolation points. Now recall that the condition number of an interpolation operator $\mathcal{I} : C(\Omega) \to C(\Omega)$, $\Omega \subset \mathbb{R}^d$, w.r.t. the L_∞-norm $\|\cdot\|_{L_\infty(\Omega)}$, is the smallest number κ_∞ satisfying

$$\|\mathcal{I}u\|_{L_\infty(\Omega)} \le \kappa_\infty \cdot \|u\|_{L_\infty(\Omega)} \quad \text{for all } u \in C(\Omega).$$

Thus, κ_∞ is the operator norm of $\mathcal{I}$ w.r.t. the norm $\|\cdot\|_{L_\infty(\Omega)}$. In the situation of polyharmonic spline interpolation, the interpolation operator $\mathcal{I}_{d,k} : C(\Omega) \to C(\Omega)$, returns, for any given argument $u \in C(\Omega)$ the polyharmonic spline interpolant $\mathcal{I}_{d,k}(u) = s_u \in C(\Omega)$ of the form (24) satisfying $s_u\big|_\Xi = u\big|_\Xi$. The following result is useful for the subsequent discussion on the stability of local interpolation by polyharmonic splines.

THEOREM 7. *The condition number κ_∞ of interpolation by polyharmonic splines is given by the Lebesgue constant*

$$\Lambda(\Omega, \Xi) = \max_{x \in \Omega} \sum_{i=1}^n |\lambda_i(x)|. \tag{36}$$

Proof. For $u \in C(\Omega)$, let $u\big|_\Xi$ be given, and let $s_u = \mathcal{I}_{d,k}(u) \in C(\Omega)$ denote the interpolant of the form (24) satisfying $u\big|_\Xi = s_u\big|_\Xi$. Using the Lagrange-type representation

$$s_u(x) = \sum_{i=1}^n \lambda_i(x) u(\xi_i)$$

of s_u, we obtain

$$\|\mathcal{I}_{d,k}u\|_{L_\infty(\Omega)} = \|s_u\|_{L_\infty(\Omega)} \le \max_{x \in \Omega} \sum_{i=1}^n |\lambda_i(x)| \cdot |u(\xi_i)| \le \Lambda(\Omega, \Xi) \cdot \|u\|_{L_\infty(\Omega)}$$

for all $u \in C(\Omega)$, and therefore $\kappa_\infty \le \Lambda(\Omega, \Xi)$.

In order to see that $\kappa_\infty \ge \Lambda(\Omega, \Xi)$, suppose that the maximum of $\Lambda(\Omega, \Xi)$ in (36) is attained at $x^* \in \Omega$. Moreover, let $g \in C(\Omega)$ denote any function satisfying $g(\xi_i) = \operatorname{sign}(\lambda_i(x^*))$, for all $1 \le i \le n$, and $\|g\|_{L_\infty(\Omega)} = 1$. Then, we obtain

$$\|\mathcal{I}_{d,k}g\|_{L_\infty(\Omega)} \ge \left(\mathcal{I}_{d,k}g\right)(x^*) = \sum_{i=1}^n \lambda_i(x^*) g(\xi_i) = \sum_{i=1}^n |\lambda_i(x^*)| = \Lambda(\Omega, \Xi)$$

and thus $\|\mathcal{I}_{d,k}g\|_{L_\infty(\Omega)} \ge \Lambda(\Omega, \Xi)\|g\|_{L_\infty(\Omega)}$. But this implies $\Lambda(\Omega, \Xi) \le \kappa_\infty$. Altogether, $\kappa_\infty = \Lambda(\Omega, \Xi)$, which completes our proof. □

The above Lemma 1 immediately yields the following important result concerning the stability of interpolation by polyharmonic splines.

THEOREM 8. *The absolute condition number of polyharmonic spline interpolation is invariant under rotations, translations and uniform scalings.*

Proof. Interpolation by polyharmonic splines is invariant under rotations and translations. It is easy to see that this property carries over to the absolute condition number. In order to see that $\kappa_\infty \equiv \kappa_\infty(\Omega, \Xi)$ is also invariant under uniform scalings, let $\Omega^h = \{hx : x \in \Omega\}$ and $\Xi^h = \{h\xi : \xi \in \Xi\}$. Then, we obtain

$$\Lambda(\Omega^h, \Xi^h) = \max_{hx \in \Omega^h} \sum_{i=1}^{n} \lambda_i^h(hx) = \max_{x \in \Omega} \sum_{i=1}^{n} \lambda_i(x) = \Lambda(\Omega, \Xi)$$

which shows that $\kappa_\infty(\Omega^h, \Xi^h) = \kappa_\infty(\Omega, \Xi)$. □

Now let us turn to the construction of a numerically stable algorithm for evaluating the polyharmonic spline interpolant s^h satisfying (27). To this end, we require that the given interpolation problem (27) is well-conditioned. Note that according to Theorem 8, this requirement depends on the geometry of the interpolation points Ξ w.r.t. the center ξ_0, but not on the scale h.

However, the spectral condition number of the matrix A_h depends on h. The following rescaling can be viewed as a simple way of preconditioning the matrix A_h for very small h. To this end, in order to evaluate the polyharmonic spline interpolant s^h satisfying (27), we prefer to work with the representation

$$s^h(hx) = < \beta_1(x), A_1^{-1} \cdot u_h >, \tag{37}$$

which immediately follows from the identity (34) and the scale-invariance of the Lagrange basis, Lemma 1. Due to (37) we can evaluate s^h at hx by solving the linear system

$$A_1 \cdot \mathbf{b} = u_h. \tag{38}$$

The solution $\mathbf{b} \in \mathbb{R}^{n+q}$ in (38) then yields the coefficients of $s^h(hx)$ w.r.t. the basis functions in $\beta_1(x)$.

By working with the representation (37) for s^h instead of the one in (28), we can avoid solving the linear system (30). This is useful insofar as the linear system (30) is ill-conditioned for very small h, but well-conditioned for sufficiently large h. The latter relies on earlier results due to Narcowich and Ward [37], where it is shown that the spectral norm of the matrix Φ_h^{-1} is bounded above by a monotonically decreasing function of the minimal Euclidean distance between the points in $h\Xi$. This in turns implies that one should, for the sake of numerical stability, avoid solving the system (30) directly for very small h. For further details on this, see [37] and the more general discussion provided by the recent paper [43] of Schaback.

4. Meshfree methods for transport problems

4.1. Transport equations

Numerical methods in flow simulation are concerned with time-dependent *hyperbolic conservation laws* of the form

$$\frac{\partial u}{\partial t} + \nabla f(u) = 0, \tag{39}$$

where for some domain $\Omega \subset \mathbb{R}^d$, $d \geq 1$, and a compact time interval $I = [0, T]$, $T > 0$, the solution $u : I \times \Omega \to \mathbb{R}$ of (39) is sought.

Moreover, $f(u) = (f_1(u), \ldots, f_d(u))^T$ denotes a given *flux tensor*, and we assume that *initial conditions*

$$u(0, x) = u_0(x), \qquad \text{for } x \in \Omega, \tag{40}$$

at time $t = 0$ are given.

One special case for (39) is *passive advection*, where the flux f is linear, i.e.,

$$f(u) = v \cdot u,$$

and thus (39) becomes

$$\frac{\partial u}{\partial t} + v \cdot \nabla u = 0, \tag{41}$$

provided that the given *velocity field*

$$v = v(t, x) \in \mathbb{R}^d, \qquad t \in I,\ x \in \Omega,$$

is *divergence-free*, i.e.,

$$\operatorname{div} v = \sum_{j=1}^{d} \frac{\partial v_j}{\partial x_j} \equiv 0.$$

For a comprehensive introduction to hyperbolic conservation laws, we recommend the textbook [28].

4.2. Semi-lagrangian advection

For the special case of passive advection, the resulting Cauchy problem (41), (40) is well-posed. In this case, the solution u is constant along the *streamlines* of fluid particles, and the shapes of these streamlines are entirely determined by the given velocity field v.

This suggests to work with a *semi-Lagrangian method* (SLM) in order to solve the Cauchy problem for passive advection. Loosely speaking, a SLM is one which follows the flow of a discrete set of particles along their streamline trajectories, and moreover the particle set is subject to dynamic changes during the simulation. Therefore, any SLM may be regarded as a special instance of the classical *method of characteristics* (MOC). Indeed, this is because the streamlines of the flow particles are the *characteristic curves* of the equation (41) [28].

In order to be more precise about the SLM, let $\Xi \subset \Omega$ denote a current finite set of nodes, at time $t \in I$, each of whose elements $\xi \in \Xi$ corresponds to a fluid particle located at ξ. Now for a fixed time step size $\tau > 0$, the advection in the SLM at time step $t \to t + \tau$ is accomplished as follows. For any node $\xi \in \Xi$, an approximation to its *upstream point* $x^- \equiv x^-(\xi)$ is computed. The upstream point x^- of ξ is the spatial location of that particle at time t, which by traversing along its corresponding streamline arrives at the node ξ at time $t + \tau$. Figure 1 shows the corresponding upstream point of a node ξ, along with its streamline trajectory.

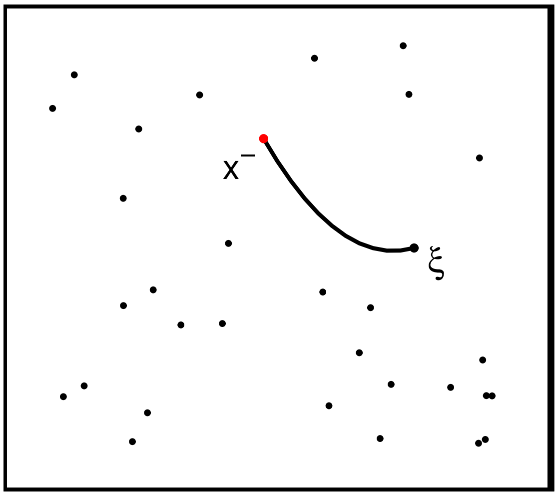

Figure 1: The point x^- is the upstream point of the node ξ.

We remark that computing the upstream point x^- of any node $\xi \in \Xi$ amounts to solving the *ordinary differential equation* (ODE)

$$\dot{x} = \frac{dx}{dt} = v(t, x) \tag{42}$$

with initial condition $x(t + \tau) = \xi$, and so $x(t) = x^-$.

Adopting some standard notation from dynamic systems, we can express the upstream point x^- of ξ as

$$x^- = \Phi^{t,t+\tau}\xi, \tag{43}$$

where $\Phi^{t,t+\tau} : \Omega \to \Omega$ denotes the *continuous evolution* of the (backward) flow of (42). An equivalent formulation for (43) is given by $\xi = \Phi^{t+\tau,t}x^-$, since $\Phi^{t+\tau,t}$ is the inverse of $\Phi^{t,t+\tau}$.

Now since the solution u of (41) is constant along the trajectories of the flow particles, we have $u(t, x^-) = u(t+\tau, \xi)$, and so the desired values $\{u(t+\tau, \xi)\}$, $\xi \in \Xi$, may immediately be obtained from the upstream point values $u(t, x^-)$. But in general, neither the *exact* location of x^-, nor the value $u(t, x^-)$ is known.

Therefore, during the performance of the flow simulation, this requires first computing an approximation $\tilde{x}$ of the upstream point $x^- = \Phi^{t,t+\tau}\xi$ for each $\xi \in \Xi$. It is convenient to express the approximation $\tilde{x}$ of x^- as

$$\tilde{x} = \Psi^{t,t+\tau}\xi,$$

where $\Psi^{t,t+\tau} : \Omega \to \Omega$ is the *discrete evolution* of the flow, corresponding to the continuous evolution $\Phi^{t,t+\tau}$ in (43) [7]. The operator $\Psi^{t,t+\tau}$ is given by any specific numerical method for solving the above ODE (42).

Having computed $\tilde{x}$, the value $u(t, \tilde{x})$ is then determined from the current values $\{u(t, \xi)\}_{\xi \in \Xi}$ by local interpolation. Altogether, the above discussion leads us to the following algorithm concerning the advection step $t \to t+\tau$ of the semi-Lagrangian method.

ALGORITHM 1. **(Semi-lagrangian advection).**

INPUT: Time step size $\tau > 0$, node set $\Xi \subset \Omega$, and values $\{u(t, \xi)\}_{\xi \in \Xi}$.

FOR each $\xi \in \Xi$ **DO**

(a) Compute the upstream point approximation $\tilde{x} = \Psi^{t,t+\tau}\xi$;

(b) Determine the value $u(t, \tilde{x})$ by local interpolation;

(c) Advect by letting $u(t+\tau, \xi) = u(t, \tilde{x})$.

OUTPUT: The values $u(t+\tau, \xi)$, for all $\xi \in \Xi$, at time $t+\tau$.

The local interpolation in step **(b)** of the above algorithm needs some comments. First note that $\tilde{x}$, the approximation of the upstream point of ξ, is not necessarily contained in the node set Ξ. Therefore, the desired value $u(t, \tilde{x})$ is to be computed from the given values $\{u(t, \xi)\}_{\xi \in \Xi}$ of u at the nodes in Ξ. This is done by local interpolation. To this end, a set $\mathcal{N} \equiv \mathcal{N}(\tilde{x}) \subset \Xi$ of neighbouring nodes of $\tilde{x}$ is determined. In order to make one concrete example, $\mathcal{N}$ could, for some suitable number n, be the set of n nearest neighbours of $\tilde{x}$ in Ξ. The given function values of $u(t, \cdot)$ at the neighbouring nodes are then used in order to solve the interpolation problem

$$u(t, \nu) = s(\nu), \qquad \text{for all } \nu \in \mathcal{N}, \tag{44}$$

by a *suitable* scattered data interpolation scheme, which outputs an interpolant $s : \Omega \to \mathbb{R}$ satisfying (44). For this purpose, we prefer to work with polyharmonic spline interpolation, so that s in (44) is required to have the form (24). The desired approximation of $u(t, \tilde{x})$ is obtained by the evaluation of s at $\tilde{x}$, so we let $u(t, \tilde{x}) = s(\tilde{x})$.

We remark that semi-Lagrangian advection schemes of the above form are unconditionally stable. This is in contrast to Eulerian schemes, which, for the sake of stability, typically work with very small time steps [28]. For a concise analysis concerning the convergence and stability of semi-Lagrangian methods, we refer to the paper [14] by Falcone and Ferretti. A more general discussion on semi-Lagrangian methods is provided in the textbooks [11, 36]; for applications of the SLM in atmospheric problems, see the review [49] by Staniforth and Côté and the seminal papers [40, 41] of Robert.

4.3. Method of backward characteristics

Now let us return to the general case of (39) where the flux function f is, unlike in (41), *nonlinear*. We remark that nonlinear cases are much more complicated than the linear one of passive advection. Therefore, the construction of a generalization to the above semi-Lagrangian method in Algorithm 1 requires particular care. Indeed, in contrast to the linear case, a nonlinear flux function f usually leads to *discontinuities* in the solution u, *shocks*, as observed in many relevant applications, such as fluid flow and gas dynamics. In such situations, the classical method of characteristics becomes unwieldy or impossible, as the evolution of the flow along the characteristic curves is typically very complicated, or characteristic curves may even be undefined (see [11, Subsection 6.3.1] for a discussion on these phenomena).

Now in order to be able to model the behaviour of the solution with respect to shock formation and shock propagation we work with a *vanishing viscosity* approach, yielding the modified *advection-diffusion equation*

$$\frac{\partial u}{\partial t} + \nabla f(u) = \epsilon \cdot \Delta u, \tag{45}$$

where the parameter $\epsilon > 0$ is referred to as the *diffusion coefficient*. In this way, the solution u of the *hyperbolic* equation (39) is approximated arbitrarily well by the solution of the modified *parabolic* equation (45), provided that the parameter ϵ is sufficiently small. This modification is a standard stabilization technique for nonlinear equations, dating back to Burgers [6], who utilized a flux function of the form

$$f(u) = \frac{1}{2}u^2 \cdot r, \tag{46}$$

with some flow direction $r \in \mathbb{R}^d$, for modelling free turbulences in fluid dynamics. The resulting *Burgers equation* is nowadays a popular standard test case for nonlinear transport equations. We come back to this test case in Subsection 5.2.

Now let us propose a meshfree advection scheme for solving the above nonlinear equation (45). Starting point for this modified approach is the discretization

$$\frac{u(t+\tau, \xi) - u(t, x^-)}{\tau} = \epsilon \cdot \Delta u(t, x^-) \tag{47}$$

of the Lagrangian form

$$\frac{du}{dt} = \epsilon \cdot \Delta u,$$

of (45), where

$$\frac{du}{dt} = \frac{\partial u}{\partial t} + \nabla f(u)$$

is the *material derivative*.

Note that the discretization in (47) allows us to work with a similar advection scheme as in the linear case, given by Algorithm 1. Indeed, having computed for any $\xi \in \Xi$ an approximation $\tilde{x} = \Psi^{t,t+\tau}\xi$ to its upstream point $x^- = \Phi^{t,t+\tau}\xi$, the desired approximation of $u(t+\tau,\xi)$ is then given by

$$u(t+\tau,\xi) = u(t,\tilde{x}) + \tau \cdot \epsilon \cdot \Delta u(t,\tilde{x}), \qquad \text{for } \xi \in \Xi.$$

However, in contrast to plain passive advection, the characteristic curves of the equation (45) depend also on u. In particular, the advection velocity $v = \frac{\partial f(u)}{\partial u}$ depends on u. This amounts to applying a more sophisticated integration scheme (compared with the one of the previous subsection) in order to compute for any $\xi \in \Xi$ its corresponding upstream point approximation $\tilde{x} = \Psi^{t,t+\tau}\xi$. For the sake of brevity, we prefer to omit these lengthy technical details, which are immaterial for the purposes of this chapter. Instead, we refer to the discussion in [3].

The following algorithm reflects the advection step $t \to t+\tau$ of the suggested method of (backward) characteristics.

ALGORITHM 2. **(Method of characteristics).**

INPUT: Time step τ, nodes Ξ, values $\{u(t,\xi)\}_{\xi\in\Xi}$, diffusion coefficient ϵ.

FOR each $\xi \in \Xi$ **DO**

- **(a)** Compute the upstream point approximation $\tilde{x} = \Psi^{t,t+\tau}\xi$;
- **(b)** Determine the values $u(t,\tilde{x})$ and $\Delta u(t,\tilde{x})$ by local interpolation;
- **(c)** Advect by letting $u(t+\tau,\xi) = u(t,\tilde{x}) + \tau \cdot \epsilon \cdot \Delta u(t,\tilde{x})$.

OUTPUT: The values $u(t+\tau,\xi)$, for all $\xi \in \Xi$, at time $t+\tau$.

Step **(b)** of Algorithm 2 deserves a comment concerning the interpolation of the value $\Delta u(t,\tilde{x})$. Similar as in Algorithm 1 we work with local interpolation by polyharmonic splines, but with a *smoother* basis function, such that the Laplacian Δs of the interpolant s satisfying (44) is everywhere well-defined. The desired approximation of $\Delta u(t,\tilde{x})$ is then obtained by $\Delta s(t,\tilde{x})$.

4.4. Adaption rules

In this section, the adaptive modification of the node set Ξ is explained. This is done after each time step $t \to t+\tau$ of the semi-Lagrangian method (Algorithm 1) in case of passive advection (41), or of the method of characteristics (Algorithm 2), when solving nonlinear advection-diffusion equations of the form (45). In either case, the *current* node values $u(t, \xi)$, $\xi \in \Xi$, are used in order to adaptively modify Ξ. Immediately before the first time step $0 \to \tau$, the nodes are first randomly chosen in Ω, before the adaption rules, to be explained below, are applied. This then yields the initial node set $\Xi \equiv \Xi(0)$.

The modification of the current node set $\Xi \equiv \Xi(t)$ (at time t) is accomplished by the removal (coarsening), and the insertion (refinement) of selected nodes, so that a modified node set $\Xi \equiv \Xi(t + \tau)$ (at time $t + \tau$) is obtained. The adaptive modification of the nodes in Ξ relies on a customized a posteriori error indicator, to be explained in the following subsection.

Error indication.

An effective strategy for the adaptive modification of the nodes requires well-motivated refinement and coarsening rules as well as a customized error indicator. We understand the error indicator $\eta : \Xi \to [0, \infty)$ as a function of the current node set $\Xi \equiv \Xi(t)$ (at time t) which assigns a *significance* value $\eta(\xi)$ to each node $\xi \in \Xi$. The value $\eta(\xi)$ is required to reflect the local approximation quality of the interpolation around $\xi \in \Xi$. The significances $\eta(\xi)$, $\xi \in \Xi$, are then used in order to flag single nodes $\xi \in \Xi$ as "to be refined" or "to be coarsened" according to the following criteria.

DEFINITION 5. *Let* $\eta^* = \max_{\xi \in \Xi} \eta(\xi)$*, and let* $\theta_{\text{crs}}, \theta_{\text{ref}}$ *be two tolerance values satisfying* $0 < \theta_{\text{crs}} < \theta_{\text{ref}} < 1$. *We say that a node* $\xi \in \Xi$ *is* to be refined*, iff* $\eta(\xi) > \theta_{\text{ref}} \cdot \eta^*$*, and* ξ *is* to be coarsened*, iff* $\eta(\xi) < \theta_{\text{crs}} \cdot \eta^*$.

In our numerical examples, typical choices for the relative tolerance values are $\theta_{\text{crs}} = 0.001$ and $\theta_{\text{ref}} = 0.1$. Note that a node ξ cannot be refined and be coarsened at the same time; in fact, it may neither be refined nor be coarsened.

Now let us turn to the definition of the error indicator η. To this end, we follow along the lines of [21], where a scheme for the detection of discontinuities of a surface, *fault lines*, from scattered data was developed. We let

$$\eta(\xi) = |u(\xi) - s(\xi)|,$$

where $s \equiv s_{\mathcal{N}}$ denotes the polyharmonic spline interpolant, which matches the values of $u \equiv u(t, \cdot)$ at a neighbouring set $\mathcal{N} \equiv \mathcal{N}(\xi) \subset \Xi \setminus \xi$ of current nodes, i.e., $s(\nu) = u(\nu)$ for all $\nu \in \mathcal{N}$. In our numerical examples for bivariate data, where $d = 2$, we work with local thin plate spline interpolation. Recall that this particular interpolation scheme reconstructs linear polynomials. In this case, the value $\eta(\xi)$ vanishes whenever u is linear around ξ. Moreover, the indicator $\eta(\xi)$ is small whenever the *local* reproduction quality of the interpolant s is good. In contrast to this, a high value of $\eta(\xi)$ typically indicates that u is subject to strong variation locally around ξ.

Coarsening and refinement

In order to obtain good approximation quality at small computational costs, we insert new nodes into regions where the value of η is high (refinement), whereas nodes from

Ξ are removed in regions where the value of η is small (coarsening).

To avoid additional computational overhead and complicated data structures, effective adaption rules are required to be as simple as possible. In particular, these rules ought to be given by *local* operations on the current node set Ξ. The following coarsening rule is in fact very easy and, in combination with the refinement, it turned out to be very effective as well.

Coarsening. A node $\xi \in \Xi$ is *coarsened* by its removal from the current node set Ξ, i.e., Ξ is modified by replacing Ξ with $\Xi \setminus \xi$.

As to the refinement rules, these are constructed on the basis of the local error estimate (17) for polyharmonic spline interpolation. The refinement of any node $\xi \in \Xi$ should aim at the reduction of the local error (17) around ξ. We accomplish this by reducing the distance function

$$d_{\mathcal{N}} = \min_{\nu \in \mathcal{N}} \| \cdot - \nu \|$$

in a local neighbourhood of ξ. In order to explain this, we need to recall some ingredients from computational geometry, in particular Voronoi diagrams [39].

For any node $\xi \in \Xi$, its corresponding *Voronoi tile*

$$V_\Xi(\xi) = \left\{ y \in \mathbb{R}^d \,:\, d_\Xi(y) = \|y - \xi\| \right\} \subset \mathbb{R}^d$$

w.r.t. the point set Ξ is a convex polyhedron containing all points in $\mathbb{R}^d$ which are at least as close to ξ as to any other point in Ξ. The boundary vertices of $V_\Xi(\xi)$, called *Voronoi points*, form a finite point set $\mathcal{V}_\xi$ in the neighbourhood of ξ. Figure 2 shows the Voronoi tile $V_\Xi(\xi)$ of a node ξ along with the set $\mathcal{V}_\xi$ of its Voronoi points.

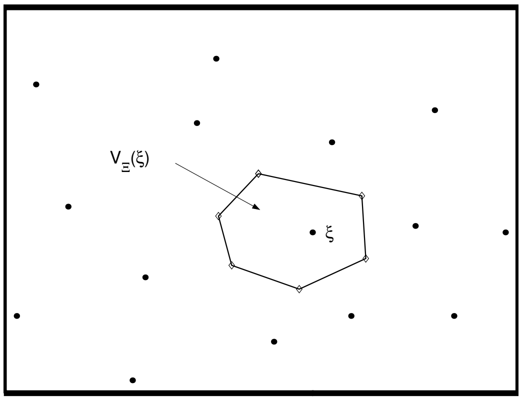

Figure 2: Refinement of the node ξ. The Voronoi points ($\diamond$) are inserted.

Now observe that for any $\xi \in \mathcal{N}$, the distance function $d_{\mathcal{N}}$ is convex on $V_\Xi(\xi)$. Moreover, the function $d_{\mathcal{N}}$ has local maxima at the Voronoi points in $\mathcal{V}_\xi$. Altogether, this gives rise to define the local refinement of nodes as follows.

Refinement. A node $\xi \in \Xi$ is *refined* by the insertion of its Voronoi points into the current node set Ξ, i.e., Ξ is modified by replacing Ξ with $\Xi \cup \mathcal{V}_\xi$.

5. Meshfree fluid flow simulation

In this section, the good performance of the proposed meshfree advection scheme is shown, where the utility of the adaptive sampling strategy is demonstrated. To this end, we work with the following two popular test case scenarios from flow simulation.

The *slotted cylinder*, subject of Subsection 5.1, is concerning passive advection. In this case, the semi-Lagrangian method (Algorithm 1) in combination with the adaption rules of Subsection 4.4 is used. The subsequent discussion in Subsection 5.2 is then devoted to the aforementioned nonlinear *Burgers equation*. In this test case, we work with the method of characteristics (Algorithm 2) in combination with the adaption rules of Subsection 4.4

5.1. The slotted cylinder: a test case for passive advection

The *slotted cylinder*, suggested by Zalesak [55], is a popular test case scenario for flow simulation concerning passive advection. In this test case, the domain $\Omega = [-0.5, 0.5] \times [-0.5, 0.5] \subset \mathbb{R}^2$ is the shifted unit square, and the initial conditions in (40) are given by

$$u_0(x) = \begin{cases} 1 & \text{for } x \in D, \\ 0 & \text{otherwise,} \end{cases}$$

where $D \subset \Omega$ is the slotted disc of radius $r = 0.15$ centered at $(-0.25, 0)$ with slot width 0.06 and length 0.22, see Figure 3 **(a)**.

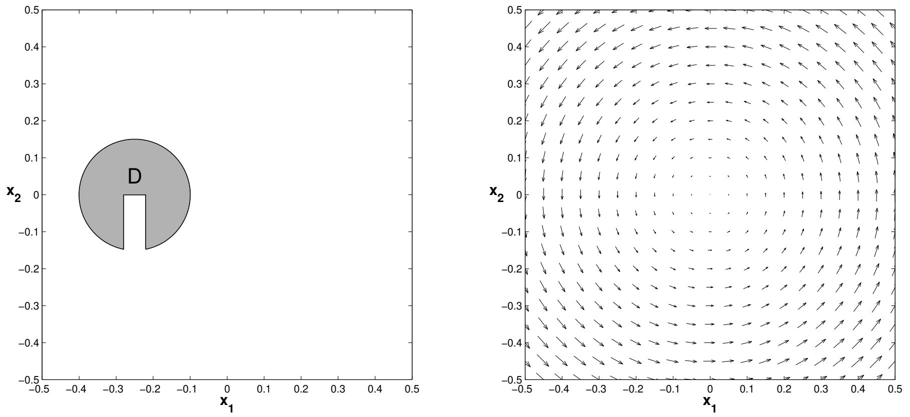

(a) **(b)**

Figure 3: The slotted cylinder. **(a)** Initial condition and **(b)** velocity field.

The slotted cylinder is rotated counter-clockwise by the steady flow field $v(x) = (-x_2, x_1)$, see Figure 3 **(b)**. Throughout the simulation, we work with a constant time step size $\tau = 0.1$, so that one revolution of the slotted cylinder around the origin requires 63 time steps. In our numerical experiment, we have recorded ten revolutions of the slotted cylinder, i.e., we let $I = [0, 629\tau]$.

Figure 6 shows the 3D view on the solution u and the corresponding node distribution during the first revolution of the slotted cylinder, at times $t_{16} = 16\tau$, $t_{32} = 32\tau$, and $t_{47} = 47\tau$. Observe that the distribution of the nodes is well-adapted to the edges of the slotted cylinder. In fact, the dense sampling along the edges leads to a high resolution of the model near the discontinuities of the solution u. On the other hand, the sparsity of the sampling in *flat* regions, where u is constant, serves to reduce the data size of the model, and thus the required computational costs. In conclusion, due to the adaptive sampling strategy, the two (conflicting) requirements of good approximation quality and computational efficiency are well-balanced.

As to the long-term behaviour of the simulation, Figure 7 shows in comparison the 3D view and the node distribution for the initial condition u_0, along with the numerical solution u obtained after five (at time $t_{315} = 315\tau$) and ten (at time $t_{629} = 629\tau$) full revolutions of the slotted cylinder. Observe that the shape of the slotted cylinder is maintained remarkably well. Moreover, numerical diffusion is widely avoided. This robust behaviour is due to the adaptive node sampling, which continues to resolve the edges of the slotted cylinder very well.

5.2. Burgers equation: a nonlinear standard test

The equation

$$\frac{\partial u}{\partial t} + u \nabla u \cdot r = \epsilon \cdot \Delta u, \tag{48}$$

was introduced in 1940 by Burgers [6] as a mathematical model of free turbulence in fluid dynamics. Burgers equation (48) is nowadays a popular standard test case for the simulation of nonlinear flow processes, and for the modelling of *shock waves*.

The nonlinear flux tensor (46) leads, in the hyperbolic equation (39), to *shocks*. As soon as the shock front occurs, there is no classical solution of the equation (39), and its weak solution becomes discontinuous. However, the modified parabolic equation (48) has for all $t > 0$ a *smooth* solution u_ϵ which approximates (for sufficiently small ϵ) the occuring shock front propagation arbitrarily well.

We use Burgers equation (48) in order to demonstrate the utility of adaptive sampling, in combination with the meshfree method of characteristics (Algorithm 2), for the modelling of shock fronts.

In the considered test case, we let

$$u_0(x) = \begin{cases} 0 & \text{for } \|x - c\| \geq R, \\ \exp\left(\frac{\|x-c\|^2}{\|x-c\|^2 - R^2}\right) & \text{otherwise,} \end{cases}$$

for the initial condition in (40), where $R = 0.25$, $c = (0.3, 0.3)$, and we let the unit square $\Omega = [0, 1]^2$ be the computational domain. Figure 4 shows the initial condition and the flow field $r = (1, 1)$, being aligned along the diagonal in Ω.

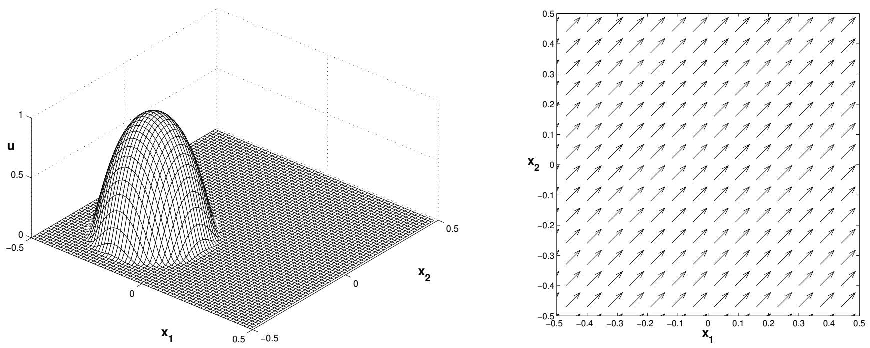

(a) **(b)**

Figure 4: Burgers equation. **(a)** Initial condition u_0 and **(b)** flow field.

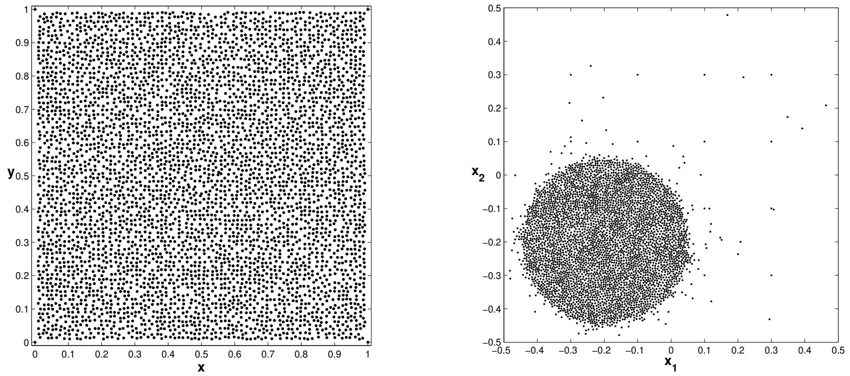

(a) **(b)**

Figure 5: Burgers equation. **(a)** Randomly chosen node set of size $|\Xi| = 4446$ and **(b)** initial node distribution comprising $|\Xi| = 1484$ nodes.

The adaptive distribution of the initial node set is shown in Figure 5 **(b)**. Recall that the construction of this node set is done by applying the adaption rules of Subsection 4.4 on a randomly chosen node set in Ω. To this end, we first selected the node set Ξ displayed in Figure 5 **(a)**, of size $|\Xi| = 4446$, by random, before the significances $\eta(\xi)$ at the nodes in Ξ are used in order to compute the initial node set $\Xi \equiv \Xi(0)$ of the simulation, shown in Figure 5 **(b)**. Observe that the adaptive distribution of the nodes in Figure 5 **(b)** manages to localize the support of the initial condition u_0 very well.

Moreover, in this simulation, a constant time step size $\tau = 0.004$ is selected, and we let $I = [0, 330\tau]$. A plot of the numerical solution u at the three time steps $t_{110} = 110\tau$, $t_{220} = 220\tau$, and $t_{330} = 330\tau$ is shown in Figure 8, along with the corresponding distribution of the nodes. Observe that the adaptive node distribution continues to localize the support of the solution u very well. This helps, on the one hand, to reduce the resulting computational costs of the simulation. On the other hand, the shock front propagation is well-resolved by the high density of the nodes around the shock, see Figure 8. Altogether, the adaptive node distribution manages to capture the evolution of the flow very effectively. This confirms the utility of the customized adaption rules yet once more.

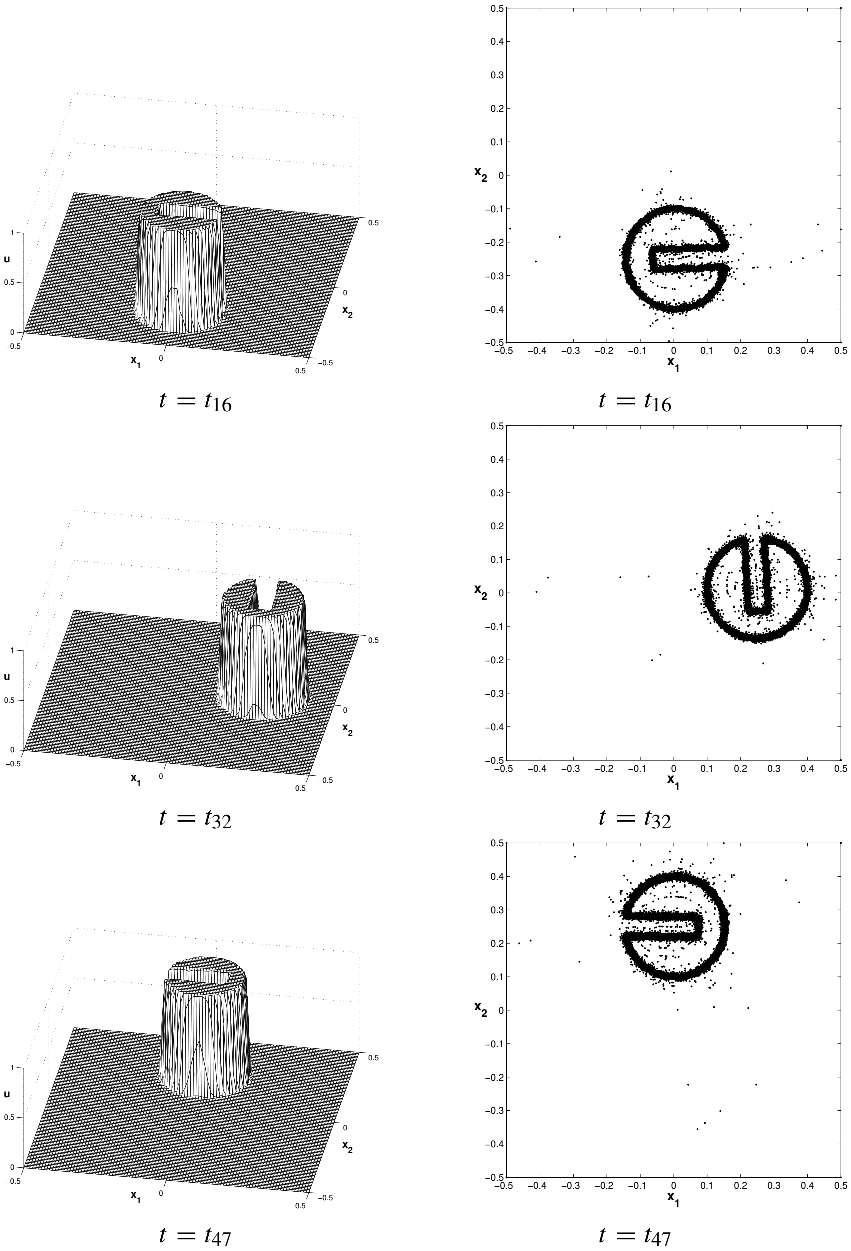

Figure 6: The slotted cylinder. 3D view on the solution u (left column) and the corresponding node distribution (right column) at time $t_{16} = 16\tau$, $t_{32} = 32\tau$, and $t_{47} = 47\tau$.

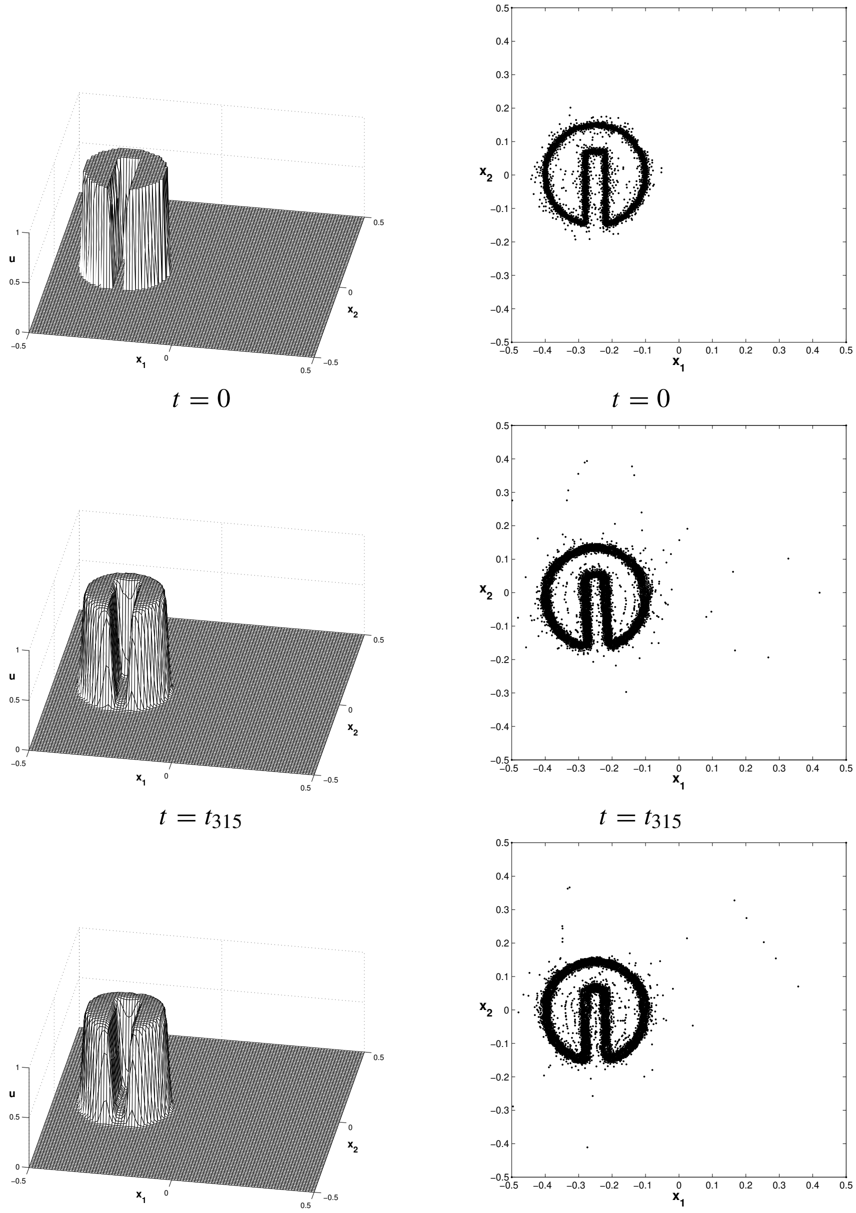

$t = 0$ $t = 0$

$t = t_{315}$ $t = t_{315}$

$t = t_{629}$ $t = t_{629}$

Figure 7: The slotted cylinder. 3D view and node distribution of the initial condition (top row), where $t = 0$, after five revolutions (middle row), at time $t_{315} = 315\tau$, and after ten revolutions (bottom row), at time $t_{629} = 629\tau$.

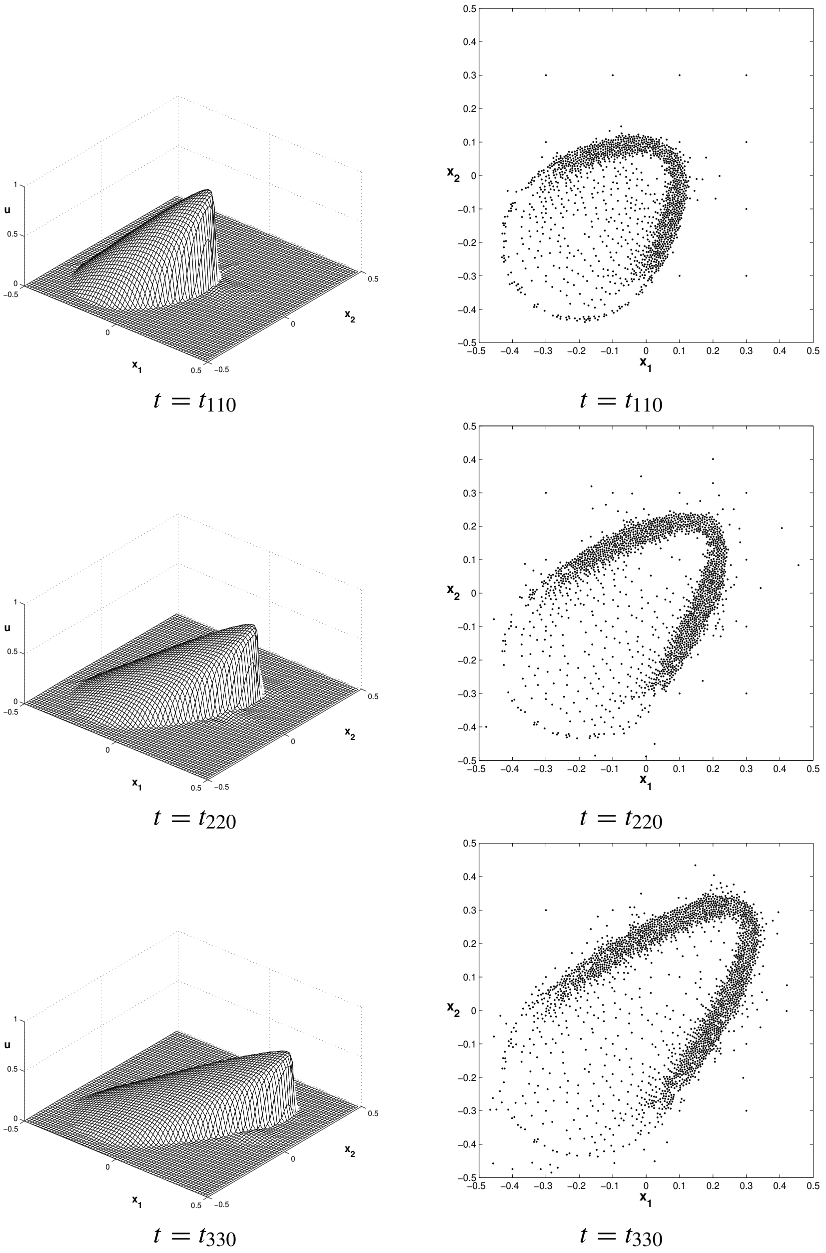

Figure 8: Burgers equation. Evolution of the solution u at three different time steps, $t_{110} = 110\tau$, $t_{220} = 220\tau$, and $t_{330} = 330\tau$ (left column), and the corresponding node distribution (right column).

References

[1] BEHRENS J. AND ISKE A., *Grid-free adaptive semi-Lagrangian advection using radial basis functions*, Computers and Mathematics with Applications **43** 3-5 (2002), 319–327.

[2] BEHRENS J., ISKE A. AND PÖHN S., *Effective node adaption for grid-free semi-Lagrangian advection*, in: "Discrete Modelling and Discrete Algorithms in Continuum Mechanics", (Eds. Sonar Th. and Thomas I.), Logos Verlag, Berlin 2001, 110–119.

[3] BEHRENS J., ISKE A. AND KÄSER M., *Adaptive meshfree method of backward characteristics for nonlinear transport equations*, in: "Meshfree Methods for Partial Differential Equations", (Eds. Griebel M. and Schweitzer M.A.), Springer-Verlag, Heidelberg 2002, 21–36.

[4] BERNSTEIN S., *Sur les fonctions absolument monotones*, Acta Mathematica **51** (1928), 1–66.

[5] BUHMANN M.D., *Radial basis functions*, Acta Numerica (2000), 1–38.

[6] BURGERS J.M., *Application of a model system to illustrate some points of the statistical theory of free turbulence*, Proc. Acad. Sci. Amsterdam **43** (1940), 2–12.

[7] DEUFLHARD P. AND BORNEMANN F., *Scientific computing with ordinary differential equations*, Springer, New York 2002.

[8] DUCHON J., *Interpolation des fonctions de deux variables suivant le principe de la flexion des plaques minces*, R.A.I.R.O. Analyse Numeriques **10** (1976), 5–12.

[9] DUCHON J., *Splines minimizing rotation-invariant semi-norms in Sobolev spaces*, in: "Constructive Theory of Functions of Several Variables", (Eds. Schempp W. and Zeller K.), Springer, Berlin 1977, 85–100.

[10] DUCHON J., *Sur l'erreur d'interpolation des fonctions de plusieurs variables par les D^m-splines*, R.A.I.R.O. Analyse Numeriques **12** (1978), 325–334.

[11] DURRAN D.R., *Numerical methods for wave equations in geophysical fluid dynamics*, Springer, New York 1999.

[12] DYN N., *Interpolation of scattered data by radial functions*, in: "Topics in Multivariate Approximation", (Eds. Chui C.K., Schumaker L.L. and Utreras F.I.), Academic Press 1987, 47–61.

[13] DYN N., *Interpolation and approximation by radial and related functions*, (Eds. Chui C.K., Schumaker L.L. and Ward J.D.), Academic Press, New York 1989, 211–234.

[14] FALCONE M. AND FERRETTI R., *Convergence analysis for a class of high-order semi-Lagrangian advection schemes*, SIAM J. Numer. Anal. **35** 3 (1998), 909–940.

[15] FASSHAUER G.E., *Solving differential equations with radial basis functions: multilevel methods and smoothing*, Advances in Comp. Math. **11** (1999), 139–159.

[16] FRANKE C. AND SCHABACK R., *Convergence orders of meshless collocation methods using radial basis functions*, Advances in Comp. Math. **8** (1998), 381–399.

[17] FRANKE C. AND SCHABACK R., *Solving partial differential equations by collocation using radial basis functions*, Appl. Math. Comp. **93** (1998), 73–82.

[18] GELFAND I.M. AND SHILOV G.E., *Generalized functions, Vol. 1: properties and operations*, Academic Press, New York 1964.

[19] GELFAND I.M. AND VILENKIN N.Y., *Generalized functions, Vol. 4: applications of harmonic analysis*, Academic Press, New York 1964.

[20] GUO K., HU S. AND SUN X., *Conditionally positive definite functions and Laplace-Stieltjes integrals*, J. Approx. Theory **74** (1993), 249–265.

[21] GUTZMER T. AND ISKE A., *Detection of discontinuities in scattered data approximation*, Numerical Algorithms **16** 2 (1997), 155–170.

[22] HIGHAM N.J., *Accuracy and stability of numerical algorithms*, SIAM, Philadelphia 1996.

[23] ISKE A., *Charakterisierung bedingt positiv definiter Funktionen für multivariate Interpolationsmethoden mit radialen Basisfunktionen*, Dissertation, Universität Göttingen 1994.

[24] ISKE A., *Scattered data modelling using radial basis functions*, in: "Tutorials on Multiresolution in Geometric Modelling", (Eds. Iske A., Quak E. and Floater M.S.), Springer-Verlag, Heidelberg 2002, 205–242.

[25] ISKE A., *On the approximation order and numerical stability of local Lagrange interpolation by polyharmonic splines*, to appear in: "Proceedings of the *5th International Conference on Multivariate Approximation*", Bommerholz 2002.

[26] KANSA E.J., *Multiquadrics - a scattered data approximation scheme with applications to computational fluid dynamics - I: surface approximations and partial derivative estimates*, Comput. Math. Appl. **19** (1990), 127–145.

[27] KANSA E.J., *Multiquadrics - a scattered data approximation scheme with applications to computational fluid dynamics - I: solution to parabolic, hyperbolic, and elliptic partial differential equations*, Comput. Math. Appl. **19** (1990), 147–161.

[28] LEVEQUE R.L., *Numerical methods for conservation laws*, Birkhäuser, Basel 1992.

[29] MADYCH W.R. AND NELSON S.A., *Multivariate interpolation: a variational theory*, manuscript, 1983.

[30] MADYCH W.R. AND NELSON S.A., *Multivariate interpolation and conditionally positive definite functions I*, Approx. Theory Appl. **4** (1988), 77–89.

[31] MADYCH W.R. AND NELSON S.A., *Multivariate interpolation and conditionally positive definite functions II*, Math. Comp. **54** (1990), 211–230.

[32] MEINGUET J., *Multivariate interpolation at arbitrary points made simple*, Z. Angew. Math. Phys. **30** (1979), 292–304.

[33] MEINGUET J., *An intrinsic approach to multivariate spline interpolation at arbitrary points*, in: "Polynomial and spline approximations", (Ed. Sahney N.B.), Reidel, Dordrecht 1979, 163–190.

[34] MEINGUET J., *Surface spline interpolation: basic theory and computational aspects*, in: "Approximation Theory and Spline Functions", (Eds. Singh S.P., Bury J.H. and Watson B.), Reidel, Dordrecht 1984, 127–142.

[35] MICCHELLI C.A., *Interpolation of scattered data: distance matrices and conditionally positive definite functions*, Constr. Approx. **2** (1986), 11–22.

[36] MORTON K.W., *Numerical solution of convection-diffusion problems*, Chapman & Hall, London 1996.

[37] NARCOWICH F.J. AND WARD J.D., *Norm estimates for the inverses of a general class of scattered-data radial-function interpolation matrices*, J. Approx. Theory **69** (1992), 84–109.

[38] POWELL M.J.D., *The theory of radial basis function approximation in 1990*, in: "Advances in numerical analysis II: wavelets, subdivision and radial basis functions", (Ed. Light W.A.), Clarendon Press, Oxford 1992, 105–210.

[39] PREPARATA F.P. AND SHAMOS M.I., *Computational geometry*, Springer, New York 1988.

[40] ROBERT A., *A stable numerical integration scheme for the primitive meteorological equations*, Atmos. Ocean **19** (1981), 35–46.

[41] ROBERT A., *A semi-Lagrangian and semi-implicit numerical integration scheme for the primitive meteorological equations*, J. Meteor. Soc. Japan **60** (1982), 319–324.

[42] SCHABACK R., *Multivariate interpolation and approximation by translates of a basis function*, in: "Approximation theory VIII, Vol. 1: approximation and interpolation", (Eds. Chui C.K. and Schumaker L.L.), World Scientific, Singapore 1995, 491–514.

[43] SCHABACK R., *Stability of radial basis function interpolants*, in: "Approximation theory X: wavelets, splines and applications", (Eds. Chui C.K., Schumaker L.L. and Stöckler J.) Vanderbilt Univ. Press, Nashville 2002, 433–440.

[44] SCHABACK R. AND WENDLAND H., *Using compactly supported radial basis functions to solve partial differential equations*, in: "Boundary Element Technology XIII", (Eds. Chen C.S., Brebbia C.A. and Pepper D.W.), WitPress, Southampton, Boston 1999, 311–324.

[45] SCHABACK R. AND WENDLAND H., *Characterization and construction of radial basis functions*, in: "Multivariate Approximation and Applications", (Eds. Dyn N., Leviatan D., Levin D. and Pinkus A.), Cambridge University Press, Cambridge 2001, 1–24.

[46] SCHABACK R. AND WENDLAND H., *Inverse and saturation theorems for radial basis function interpolation*, Math. Comp. **71** (2002), 669–681.

[47] SCHOENBERG I.J., *Metric spaces and positive definite functions*, Trans. Amer. Math. Soc. **44** (1938), 522–536.

[48] SCHOENBERG I.J., *Metric spaces and completely monotone functions*, Annals of Mathematics **39** (1938), 811–841.

[49] STANIFORTH A. AND CÔTÉ J., *Semi-Lagrangian integration schemes for atmospheric models – a review*, Mon. Wea. Rev. **119** (1991), 2206–2223.

[50] WENDLAND H., *Piecewise polynomial, positive definite and compactly supported radial functions of minimal degree*, Advances in Comp. Math. **4** (1995), 389–396.

[51] WENDLAND H., *Meshless Galerkin methods using radial basis functions*, Math. Comp. **68** (1999), 1521–1531.

[52] WIDDER D.V., *An introduction to transform theory*, Academic Press, New York 1971.

[53] WU Z., *Multivariate compactly supported positive definite radial functions*, Advances in Comp. Math. **4** (1995), 283–292.

[54] WU Z. AND SCHABACK R., *Local error estimates for radial basis function interpolation of scattered data*, IMA J. Numer. Anal. **13** (1993), 13–27.

[55] ZALESAK S.T., *Fully multidimensional flux-corrected transport algorithms for fluids*, J. Comput. Phys. **31** (1979), 335–362.

[56] *Special issue on radial basis functions and partial differential equations*, (Eds. Kansa E.J. and Hon Y.C.), Comput. Math. Appl. **43** (2002).

AMS Subject Classification: 65D15, 65M25.

Armin ISKE
Zentrum Mathematik
Technische Universität München
D-85747 Garching, GERMANY
e-mail: `iske@ma.tum.de`